1966

A study of conduction mechanisms in thin tantalum pentoxide

Renato Abdon Rodriguez Jr.
Lehigh University

A STUDY OF CONDUCTION MECHANISMS IN THIN TANTALUM PENTOXIDE

by

Renato Abdon Rodriguez, Jr.

A Thesis

Presented to the Graduate Faculty

of Lehigh University

in Candidacy for the Degree of

Master of Science

Lehigh University

1966

Certificate of Approval

This thesis is accepted and approved in partial fulfillment of the requirements for the degree of Master of Science.

May 19, 1966
Date

Professor in Charge

Head of the Department
of Metallurgical Engineering

ACKNOWLEDGEMENTS

The author would like to express his appreciation to Dr. G. P. Conard, II, and Dr. R. N. Tauber of the Metallurgy Department for their guidance and helpful suggestions during the course of this work and to Dr. E. J. Shaw of the Princeton Research Center, Western Electric Company, for valuable consultation and general advice.

Sincere appreciation is also expressed to Dr. C. Altman and Dr. W. R. Samaroo for their helpful advice.

The author would like to thank Mr. H. Y. Kumagai for the specimens used in this thesis and to acknowledge the assistance of Mr. R. M. Higgins and Mr. M. A. DeAngelo in the preparation of the final test specimens. He would also like to thank Mr. W. J. Yost for his assistance and contributions in the laboratory.

Gratitude is expressed to his family for their understanding and tolerance during the period of thesis preparation.

TABLE OF CONTENTS

	Page
List of Figures	v
List of Tables	vii
ABSTRACT	1
I. INTRODUCTION	2
A. Previous Work	2
B. Purpose of This Study	3
II. THEORETICAL CONSIDERATIONS	4
A. Schottky Emission	4
B. Fowler-Nordheim Emission	5
C. Space Charged Limited Currents	6
D. Mead's Theory	11
III. EXPERIMENTAL PROCEDURE	13
A. Considerations in the Design of the Experiment	13
B. Specimen Description	15
C. Specimen Preparation	15
D. Environmental Equipment	16
E. Temperature Measurement and Control	17
F. Electrical Measurements	17
G. Testing Procedure	17
IV. EXPERIMENTAL RESULTS AND DISCUSSION	19
A. Fit of Data to a Space Charge Limited Model	20
B. Fit of the Data to a Schottky Model	23
C. Fit of the Data to a Fowler-Nordheim Model	24
D. Fit of the Data to Simultaneous Thermionic and Tunneling Emission	27
E. Fit of the Data to Mead's Model	27
F. Summary	28
V. SUGGESTIONS FOR FURTHER WORK	30
A. Anomalous Capacitance Effect	30
B. Relaxation Effects	31
C. Irreversible Conductivity Change	31
VI. TABLE OF SYMBOLS	67
VII. BIBLIOGRAPHY	68
VIII. VITA	70

LIST OF FIGURES

Figure — Page

1. The Space Charge Limited Triangle 42

2. Experimental Specimen in Various Stages of Preparation 43
   - A. As sputtered
   - B. Etched
   - C. Anodized
   - D. Counter electrode evaporated

3. Cross Section of Environmental Chamber 44

4. Environmental Equipment 45

5. Ramp Generator Schematic 46

6. Experimental Equipment 47

7. Holding Fixture 48

8. Block Diagram of Test Equipment 49

9. Effect of Temperature on SCL Characteristic Curve 50

10. J vs. F for 50 Å 51

11. J vs. F for 150 Å 52

12. J vs. F for 450 Å 53

13. J vs. F for 1350 Å 54

14. Schottky plot for 50 Å 55

15. Schottky plot for 150 Å 56

16. Schottky plot for 450 Å 57

17. Schottky plot for 1350 Å 58

18. Fowler-Nordheim plot for 50 Å and 1350 Å at 380°K 59

19. Fowler-Nordheim plot for 50 Å at 290°K 60

20. Fowler-Nordheim plot for 50 Å 61

LIST OF FIGURES (Cont.)

		Page
21.	Fowler-Nordheim plot for 150 $\AA^{o}$	62
22.	Fowler-Nordheim plot for 450 $\AA^{o}$	63
23.	Fowler-Nordheim plot for 1350 $\AA^{o}$	64
24.	Plot of the Data at 380^{o}K to Mead's High Temperature Theory	65
25.	Anomalous Capacitance Behavior	66

LIST OF TABLES

Table | Page

I - Tantalum Thicknesses as Deposited 32

II - Maximum Values of Test Voltages 33

III - Experimental and Calculated Data 34

IV - Slopes of Schottky Plots 39

V - Intercepts from Fowler-Nordheim Plots 40

VI - Observed and Calculated Capacitance for Samples 41

ABSTRACT

A study was made of electronic conduction mechanisms in thin tantalum oxide films anodically formed on sputtered beta tantalum. Films of thicknesses ranging from 50 Å to 1350 Å were tested over a range of temperatures from 100°K to 380°K and a range of fields from 10^6 volts/meter to 250 x 10^6 volts/meter. The data was compared to four models for limiting mechanisms for electronic conduction in insulators. These were:

1. space charge limiting
2. trap excitation mechanisms
3. Schottky thermionic emission
4. Fowler-Nordheim tunneling.

The data was analyzed qualitatively and found to fit the space charge limiting theory. The data was analyzed quantitatively and found not to fit the models proposed for trap excitation, thermionic emission, and tunneling. Therefore, it was concluded that current limiting in the samples studied was due to space charge effects.

I. INTRODUCTION

The object of this work is to study the conduction mechanism in tantalum oxide anodically formed on beta tantalum.

Oxide films on beta tantalum have not been previously studied to determine a conduction mechanism, although several workers have worked on oxide films on other materials, notably aluminum and BCC tantalum.

A. Previous Work

The first reported work was by Mead[1] working with both aluminum oxide and tantalum oxide. A conduction mechanism due to tunnel emission from the cathode to the anode was reported. Fisher and Giaever[2] reported tunneling in aluminum oxide films 40 Å to 80 Å thick with aluminum counter electrodes.

Emtage and Tantraporn[3] observed currents in aluminum and germanium oxides which were limited by Schottky emission and suggested that the data reported by Mead[1] could be fitted better to a Schottky plot than to a Fowler-Nordheim plot (see the section on conduction theories for the significance of these plots). Standley and Maissel[4] also reported a Schottky behavior for tantalum oxide above 0°C but their data departs from this behavior at lower temperatures.

Mead[5] conducted experiments on tantalum oxide and reported a current limiting mechanism due to the bulk properties of the oxide.

Finally, Lampert[6], drawing on experimental work by Rose[7] on cadmium slufide, suggested that currents in insulators might be

due to space charge limiting modified by the presence of traps in the insulator.

Other mechanisms which might be considered but which have been rejected by previous workers are ionic conduction and flaws in the oxide. Mead[5] and Maissel[4] found that the probability of a flaw occurring under a contact was reduced if a sufficiently small contact area was used. Presence of such a flaw could be detected by a linear voltage-current dependence with a positive temperature coefficient of resistance. Ionic conductivity was rejected because of the absence of matter transport associated with such a mechanism and the absence of transient effects typical of the low mobility of ionic carriers.

B. Purpose of this Study

It is obvious from the previous work in this field that there are conflicting reports on the conduction mechanism in oxides, notably Maissel's and Mead's results on bulk tantalum and sputtered tantalum. This lack of acceptance of a unique conduction mechanism for oxides suggests that the dominant conduction mechanism might vary for oxides formed on different materials or by different processes. Therefore, the conduction mechanism in tantalum oxide formed on beta tantalum was selected to be studied to determine what the dominant conduction mechanism might be.

II. THEORETICAL CONSIDERATIONS

The conduction mechanisms proposed can be divided into two categories: emission limited theories and bulk oxide property theories. Emission limited theories assume the current is limited by some mechanism determined by the interface between the metal emitter and the oxide. Bulk oxide theories assume there is an essentially inexhaustible reservoir of carriers at the interface and that the current is limited by some physical mechanism active in the bulk of the oxide.

The two emission limited mechanisms that have been suggested are Schottky emission and Fowler-Nordheim emission.

A. Schottky Emission

Schottky emission is a field-enhanced, thermionic emission described by the following relation:[8]

$$J_S = A\,T^2 \exp\left\{-e\left[\phi - \tfrac{1}{2}\,(eF/\pi\epsilon)^{\frac{1}{2}}\right]/kT\right\} \qquad (1)$$

J_S = Schottky current

A = Richardson's constant

T = Absolute temperature

e = charge of an electron

ϕ = work function of the interface

F = field strength

ϵ = permittivity of material

k = Boltzman's constant

This can be expressed for tantalum-tantalum oxide as

$$J_s = J_{so} \exp \left[.0956 \ (F)^{\frac{1}{2}}/T\right] \qquad (2)$$

where the units are mks and

$$J_{so} = A \ T^2 \ \exp \left[-e\phi/kT\right] \qquad (3)$$

The value used for the dielectric constant is 21 as determined by Klerer for oxide formed on beta tantalum.(9)

It is obvious that if a current is Schottky emission limited a plot of log J vs. $(F)^{\frac{1}{2}}$ will be a straight line with a slope of $\frac{.0415}{T}$ This is the Schottky plot.

B. Fowler-Nordheim Emission

Fowler-Nordheim emission is tunneling from the conduction band of the metal to the conduction band of the insulator. The expression for this behavior is given by Good and Muller(10) as:

$$J_F = \left[e^3F^2/8\pi h\phi t^2(y)\right] \exp- \left\{(8\pi \left[2m\right]^{\frac{1}{2}}\phi^{\frac{3}{2}})v(y)/3heF)\right\} \qquad (4)$$

where

J_F = tunneling current

h = Planck's constant

m = mass of an electron

$y = (e^3F)/\phi$

v(y) = Nordheim elliptic function

$t(y) = v(y) - 2 \ v' \ (y)/3$

and the other variables are as previously defined. For mks units this becomes

$$J_F = [1.54x10^{-10}F^2/t^2(y)\phi] \exp-[6.83x10^9\phi^{\frac{3}{2}}v(y)/F] \qquad (5)$$

where $y = 3.79 \times 10^{-5}(F)/\phi$

This can be expressed as

$$J_F = BF^2 \exp(C/F) \qquad (6)$$

where B and C are considered constants. The functional dependence of t(y) and v(y) on F is neglected because t(y) varies from 1.0 to 1.1 as y varies from 0 to 1 and v(y) varies from 1.0 to .7 as y varies from 0 to .5. The presence of tunneling as the principal current limiting mechanism could be detected by plotting log (J/F^2) vs. 1/F to see if a straight line was obtained. This is the Fowler-Nordheim plot. It should be noted that there is no explicit temperature dependence of the tunneling current. However, a temperature dependence for tunneling could be accounted for by a consideration of the effect of temperature upon ϕ, the work function.

The above analysis suggests that emission limited mechanisms can be differentiated by determining the voltage dependence of the current. A plot of log J vs. $(F)^{\frac{1}{2}}$ will be a straight line if thermionic emission predominates. A plot of log (J/F^2) vs. 1/F will be a straight line if tunneling predominates.

The bulk limiting mechanisms, assume that the interface between the metal and the oxide is an ohmic contact and therefore is an infinite reservoir of carriers.

C. Space Charge Limited Currents

The space charge limited theories are based upon the fact that

the carriers injected into the insulator are uncompensated and therefore represent a space charge. This space charge serves to limit the current in accordance with Child's law.[8] Lampert[6] shows the current will be dependent upon the second power of voltage for a perfect insulator.

$$J_{sc} = 9 \mu \epsilon F^2/8d \qquad (7)$$

J_{sc} = space charge current

μ = mobility of carrier

ϵ = permittivity of material

F = field

d = interplanar spacing of electrodes

This expression must be modified to account for the presence of traps which occur in the insulator. These traps in the insulator will immobilize some of the injected charge. This immobile charge will contribute to the space charge but not to the current. Therefore, equation (7) must be modified to take account of the effect to traps in the material. These trap sites might all occur at a single discrete energy level or they might be distributed over a range of energies. The equation for a single trapping level is given by Lampert[6] for shallow traps as:

$$J_{TSC} = [\theta/(\theta+1)] \mu \epsilon F^2/d \qquad (8)$$

J_{TSC} = current with shallow traps

$$\theta = n_c/n_t = (N_c/N_t) \exp [(E_t - E_c)/kT] \qquad (9)$$

n_c = number of carriers in conduction band

n_t = number of carriers in trapped states

N_c = effective density of states in the conduction band

N_t = density of traps

E_t = energy level of traps

E_c = energy level of conduction band

All the other symbols are as previously defined. The effect of the shallow traps is to reduce the current in the insulator with traps below that of the perfect insulator by the factor $\theta/(\theta+1)$.

Rose[7] shows that other expressions may be developed for the case where the traps are distributed in energy rather than all at the same energy level. For an even energy distribution of traps, $N_t(E)$, he finds

$$J_T = (F\mu e/d^2)N_c \exp\left[(E_c-E_f)/kT\right] \exp\left[\alpha F\right] \qquad (10)$$

where

$$\alpha = \epsilon / \left[dN_t(E)\ ekT\right] \qquad (11)$$

Lampert[6] shows that as charge is injected the Fermi level in the insulator shifts. This shift in the Fermi level occurs for the following reason. The Fermi level in the material is defined by the relation

$$n_c = N_c / \left\{1+ \exp\left[(E_c-E_f)/kT\right]\right\} \qquad (12)$$

All symbols are as previously defined. The total number of carriers in the conduction band is given by

$$n_c = n_o + n_i \tag{13}$$

n_c = total number of carriers in the conduction band

n_o = equilibrium number of thermally generated carriers

n_i = carriers injected into insulator due to the applied field

As n_i increases the Fermi level must shift up in energy to compensate for the increased number of carriers in the conduction band. If the Fermi level passes through a trap level, an abrupt increase in current will be observed. This current can be shown to be dependent upon some higher power of field, but the exact exponent has not been determined.

The behavior of a material acting in accordance with this theory was described by Lampert[6] in terms of Figure 1. In a perfect material two types of behavior might be expected. At low fields the injected charge will be small and conduction will be due to thermally generated carriers. This will result in an ohmic behavior as shown by curve I. As charge is injected, space charge effects will begin to appear and a transition to the square law behavior of equation (7) will occur. This behavior is given by curve II. The intersection of curve I and II defines a transition voltage. This is the point were the injected carriers in the conduction band and the thermally generated carriers are equal and is given by

$$F_{TR} = (ed/\epsilon)N_c \exp\left[(E_f - E_c)/kT\right] \tag{14}$$

where

F_{TR} = transition field

and all other symbols are as previously defined.

The presence of traps in the material modifies the behavior in two fashions. First it delays the transition from ohmic to square law behavior. This occurs because a portion of the injected charge is immobilized in the traps, reducing the injected charge in the conduction band. The result is the voltage at which the injected carriers and thermally generated carriers are equal is increased by the factor $1/\theta$, as given in equation (9) which gives a transition voltage of

$$F'_{TR} = (ed/\epsilon)N_t \exp\left[(E_f - E_t)/kT\right] \qquad (15)$$

The other effect of the traps is to produce a sharp increase in current with field when the traps become filled, as shown by curve III in Figure 1. When the traps fill all additional injected carriers are available in the conduction band, resulting in an abrupt increase in current. The field at which the traps become filled is given by Lampert[6] as

$$F_{TFL} = eN_t d/\epsilon \qquad (16)$$

and corresponds to the intersection of ohmic curve I and the exponential curve III of Figure 1.

As more charge is injected, the material once again becomes space charge limited and conduction returns to a square law behavior of curve II.

D. Mead's Theory

Mead[5] proposes that the conduction mechanism is limited by one of four processes, depending upon the conditions of temperature and field. He suggests that at low temperatures and low fields tunneling from the metal to the conduction band of the oxide does occur as reported by Fisher and Giaever[2]. For other conditions of temperature and field, various mechanisms occurring in the bulk of the oxide are proposed.

At high temperatures and low fields he proposes that conduction is by thermally excited electrons jumping from one isolated state to another. This mechanism yields an ohmic characteristic, exponentially dependent on temperature.

At low temperatures and high fields, he suggests that current flow is limited by field ionization of trapped electrons into the conduction band. This mechanism is discussed by Chynoweth[11]. The behavior is described by the relation

$$J = \left[e^3F^2/8\pi h\psi t^2(y)\right] \quad \exp-\left\{\left[8\pi(2m)^{\frac{1}{2}}\psi^{\frac{3}{2}}\right] v(y)/(3heF)\right\} \tag{17}$$

where

ψ = depth of the traps below the conduction band

and all other symbols are as previously defined. This relation is the same as equation (4) for the Fowler-Nordheim model for tunneling at the oxide-metal interface except the energy barrier is now ψ rather than ϕ.

At high fields and high temperatures, the rate limiting step is field enhanced, thermal excitation of trapped electrons into the

conduction band. This process is known as the Poole-Frenkel effect[12]. This behavior is described by the relation

$$J = C\,F\,\exp\left\{-e\left(\psi - \left[eF/\pi\epsilon\right]^{\frac{1}{2}}\right)/kT\right\} \qquad (18)$$

C = constant, characteristic of the process.

The difference between the mechanisms suggested by Mead[5], the tunneling mechanism of Giaever[2], and the Schottky emission mechanism of Maissel[4] is the source of the electrons. Mead considers filled trap sites in the oxide as the source of electrons, with conduction limited by the excitation process from the sites. Maissel and Giaever consider the metal as the source of electrons with conduction being limited by the excitation process across the metal-oxide interface.

III. EXPERIMENTAL PROCEDURE

A. Considerations in Design of the Experiment

The design of the experiment to determine the conduction mechanism required that provision be made to vary the voltage, temperature, and thickness of the test specimen.

The selection of a method of voltage control was governed by the following consideration. The specimen to be tested was electrically a capacitor with a time constant of the order of magnitude of 10-20 seconds. DC testing would require extremely long waiting periods to permit charging currents to decay to levels where the leakage currents could be accurately measured. This presented two problems. The first was the undesirability of the long times itself, because of the possibility of damage to the oxide at the higher current and voltage levels due to internal heating, and the greater stability required of the temperature controller because of the longer testing time at a given temperature. The second was that DC testing would require point by point recording of data with the possibility of missing significant effects by a poor choice of points.

It was decided to use a ramp voltage with time. The current-voltage relationship could then be plotted electronically. The linear nature of the voltage change would cause the charging current to be constant, and this could simply be subtracted from the total current. Finally, the possibility of damage to the oxide would be reduced because the time at the higher voltages and currents would be significantly reduced.

The control of temperature was obtained by building a low temperature chamber capable of obtaining temperatures between 77°K and 400°K. 400°K was the highest temperature to be used since Young[13] reported the film remained amorphous below this temperature and Vermilyea[14] demonstrated there was no significant thermal oxide growth below this temperature. Temperature measurement was made separately by means of a thermocouple which reduced the demands on the stability of the controller. It was only necessary to hold the temperature for the short period of time (approximately thirty seconds) necessary to make one sweep of the ramp generator. Temperature measurement could be made during this time by the independent thermocouple, giving a good temperature determination. Temperature points were selected to give approximately equal intervals on both a logarithmic and a reciprocal scale.

It was necessary to control the moisture adsorbed on the surface of the oxide since Schwartz[15] had demonstrated that it could have a significant effect on the conduction. The effect was minimized in two ways. First by heating the specimen to 130°C prior to test to drive off adsorbed moisture. Second, by the polarity of the applied voltage. Schwartz noted that, if the tantalum was negative with respect to the other electrode, the effect of adsorbed moisture was almost completely eliminated. Therefore, this polarity was selected for the test.

The specimen preparation was governed by the following considerations. All the specimens were placed upon one slide to reduce differences due to preparation of the slide, either in sputtering,

anodization, or counter electrode fabrication. The thickness of the oxide was determined by the anodization constant. The thicknesses used were selected to give equal intervals on a logarithmic scale.

B. Specimen Description

The experimental work of this thesis was done on tantalum pentoxide, anodically formed on sputtered beta tantalum. A counter electrode of gold was evaporated over the oxide. Electrical contact was made to the gold and to the tantalum. The size of the gold contacts was 2.3 x .575 mm. which gave a contact area of 1.321 square millimeters. The slide was divided into five parts of 50, 150, 450, 1350 and 4050 $\mathring{A}$ oxide thickness, and six gold electrodes were formed on each part except for the 50 $\mathring{A}$ section which had eight electrodes. Figure 2 shows the various stages in the preparation of the specimen.

C. Specimen Preparation

$1\frac{1}{2}$ x 3 inch slides of 7059 glass had beta tantalum sputtered on them in the In-Line IV machine at the Princeton Research Center. Sputtering conditions were 4 KV at 800 ma. in an atmosphere of 50 microns of argon. The thickness obtained was approximately 6000 $\mathring{A}$ tantalum. Exact figures for each of the specimens are given in Table I. Thickness of the tantalum was verified by beta back scatter and Talysurf measurements. The tantalum was verified as being the beta phase by X-ray diffraction patterns.

After sputtering, the slides were electrolytically etched to give a suitable pattern for further work. The pattern after etching

is shown in Figure 2-B. A photoresist of KMER was used to protect the pattern. The etching medium was lithium chloride in methanol.

Following the etching, the slide was anodized in five steps. The anodization voltages were 3, 9, 27, 81 and 243 volts. The entire slide was anodized at 3 volts, withdrawn 13.7 mm., anodized at 9 volts, withdrawn 12 mm., and the process continued until all five thicknesses of oxide had been formed. The anodization was done at a constant current of 35 ma. to the voltage necessary to give the desired thickness and then at constant voltage until the current was 10 ua. or less. The slide, after anodization, is shown in Figure 2-C. The thickness of the films was determined by use of the anodization constant for beta tantalum of 16 A/volt as determined by Klerer[9].

The gold counter electrodes were evaporated in a bell jar vacuum system. The slides were placed in the chamber which was evacuated to 10^{-6} mm. of Hg or less. The slide was heated to 150°C to outgas the surface and improve the adhesion of the gold. Then the gold was evaporated. This completed the preparation of the slides which were then ready for testing. The completed slide is shown in Figure 2-D.

D. Environmental Equipment

The equipment used in the experiment consisted of a double-walled copper-stainless steel chamber which held the specimen during the test. This chamber was held in a Dewar which contained liquid nitrogen. The inner wall of the chamber was wrapped with a heater which was controlled by the temperature regulator to maintain the desired tem-

perature. Figure 3 shows a cross-section and Figure 4 a photograph of the environmental equipment. The inner chamber was filled with nitrogen under a positive pressure at a flow rate of 50 cc/min. to eliminate condensation effects during the test. The nitrogen was 99.95% pure with a dew point of $-90^{o}F$ as determined by the supplier.

E. Temperature Measurement and Control

Temperatures were measured by means of copper-constantan thermocouple and a Leeds & Northrop 8690 potentiometer. The thermocouple was calibrated against a platinum resistance thermometer in the range from $-70^{o}C$ to $130^{o}C$ and against a liquid nitrogen bath for the low temperature. The liquid nitrogen used for the calibration was 99.95% pure with 10 ppm O_2, 1 ppm CO_2 as determined by the supplier.

F. Electrical Measurements

A ramp generator was used to apply voltage to the test specimen. A schematic diagram of the ramp generator is shown in Figure 5. The voltage across the specimen was measured by a HP 412 AR VTVM and the current through the specimen was measured with a HP 425 micromicroammeter. The recorder output of each of these instruments was used to drive the x-axis and y-axis respectively of a Houston Laboratories x-y recorder to give a permanent record of the results. The equipment used for the measurements is shown in Figure 6 and the specimen holding fixture in Figure 7.

G. Testing Procedure

The specimen under test was placed in the holding fixture in the

environmental chamber which was then flushed with nitrogen and heated to 130°C to drive off adsorbed moisture. Then it was brought to the temperature of the test. Each sample on the slide was alternately connected to the ramp generator and recording equipment as shown in Figure 8. The voltage and current were recorded on the x-y recorder. Upon completion of testing at one temperature a new temperature was selected or testing was terminated. When testing was terminated the specimen was placed in a desiccator for storage. When testing was resumed the specimen was again heated to 130°C before any tests were made.

IV. EXPERIMENTAL RESULTS AND DISCUSSION

Preliminary tests were made on several samples to establish the range of currents and voltages to be expected and the capabilities of the measuring equipment. During the prove-in it was noted that currents in the 4050 Å specimen could be measured only at the highest temperature of the experiment. Therefore, no data are reported on this thickness.

It was observed that the behavior of the specimen was permanently changed if the field exceeded a critical value. Exceeding the maximum voltage produced a permanent shift in the current-voltage characteristic. The direction of the shift was not unique, sometimes it was to the left and sometimes to the right. The range of voltages used in the test was restricted to values below those at which changes occurred so that changes in the behavior of the specimens could be ascribed to the independent parameters. Maximum thickness of the test are given in Table II.

When these preliminary studies were completed a new slide was selected for experimental measurements. Study of the results revealed that the behavior of all specimens of each thickness was similar. Therefore, typical samples of each thickness were selected for further analysis. The data for the samples analyzed are shown in Table III. The analysis was conducted to determine which of the following four models best explained the behavior of the material.

The models considered in analyzing the data were:

1. Schottky emission

2. Fowler-Nordheim emission

3. Trap excitation

4. Space charge limiting

The applicability of a particular model was determined by comparing the experimental data to the prediction of the model.

When the data were fitted to the predictions of each of the four models, it was found that the space charge limited model gave the best fit. The analysis for each of the models is as follows:

A. Fit of the Data to a Space Charge Limiting Model

The experimental data were compared to the current-voltage characteristic predicted by a space charge limiting theory of conduction. The theory predicts a current-voltage characteristic for an insulator as shown in Figure 9. Four distinct regions occur in the characteristic. At low fields the behavior is ohmic, i.e., J is proportional to F. This is region I. The ohmic behavior occurs because the carriers in the conduction band are independent of field since they are principally thermally generated, i.e., n_o, the thermally generated carrier density, is much larger than n_i, the injected carrier density. As the field is increased the number of injected carriers will increase. As n_i becomes larger, space charge effects will become noticeable and a transition from ohmic to square law behavior will occur. When n_i is much larger than n_o, the current will be space charge limited and J will be proportional to F^2. This is region II.

The curves in region I and II on Figure 9 are the asymptotes to the ohmic and the square law behavior. Their intersection is the point where n_o and n_i are equal and is given by Lampert[6] as

$$F'_{TR} = (ed/\epsilon)N_t \exp\left[(E_f - E_t)/kt\right] \qquad (19)$$

As the field is further increased, the traps in the insulator will become filled. When this occurs, the charge injected by further increase in field is all available for conduction. Therefore, the current will increase as some high power of the field, i.e., J will be proportional to F^{n}[6]. The value of the exponent is dependent upon the density of traps and their distribution in energy. This is region III on Figure 9. The intersection of the asymptote to this curve and the ohmic curve of region I is given by Lampert[6] as

$$F_{TFL} = e\, N_t\, d/\epsilon \qquad (20)$$

As the field is further increased the current again becomes space charge limited and J is again proportional to F^2 as shown in region IV of Figure 9.

The data obtained in this study did not cover a wide enough range of field for any one sample to display the full characteristic. The range of data was limited because at high temperatures the specimens failed at the higher fields. At low temperature the currents at the low fields could not be measured.

A satisfactory fit of the data to the predicted characteristic was obtained by considering the effect of temperature on the characteristic. The base line of the characteristic is the ohmic

behavior of region I, Figure 9. A decrease in temperature will cause the line to shift down as shown by the characteristic for T_2. Equation (19) shows the transition voltage, F'_{TR} will shift to the left with decreasing temperature. This is also shown for T_2 on Figure 9. F_{TFL} is shown by equation (20) to be temperature independent. For lower temperatures the characteristic will be as shown in Figure 9. This family of characteristics suggests that the behavior of a specimen would exhibit a transition from a first order behavior at high temperatures to second order, then to higher order and returning to second order with successively lower temperatures. Consider a specimen operating in the current range from J_1 to J_2 on Figure 9. At T_1 its behavior is ohmic. At T_2 it would exhibit a transition from ohmic to square law. At T_3 it would exhibit a transition from square law to higher order. At T_4 and T_5 it would exhibit a higher order behavior.

Consideration of each of the specimens shows exactly this change of type of behavior with decreasing temperature.

The 50 $\overset{o}{A}$ film in Figure 10 shows an ohmic behavior at $380^{o}K$. At $290^{o}K$, it is operating in the transition region where the current is changing from an ohmic to a square law dependence on voltage. At the highest temperatures, it is operating in the region where the current has a high order dependence on voltage.

The 150 $\overset{o}{A}$ film in Figure 11 shows the ohmic behavior at $380^{o}K$. It is operating in the transition region from ohmic to square law dependence on voltage at $290^{o}K$. At the highest temperatures, the current has a high order dependence on voltage.

The 450 Å film in Figure 12 is operating in the transition region from ohmic to square law behavior at 380°K. It is in the transition region from square law behavior to a high order voltage dependence at 290°K. At 214°K and 148°K, it is operating in the region of higher order dependence of current on voltage. At 114°K and 101°K, it shows the transition from higher order dependence of current back to a square law dependence.

The 1350 Å film in Figure 13 shows the ohmic behavior at 380°K and the transition from higher order dependence of current on voltage to a second order dependence.

B. Fit of Data to a Schottky Model

In the case of the Schottky model the best comparison is obtained by plotting log J vs. $(F)^{\frac{1}{2}}$. The Schottky model as shown in equation (2) predicts the following voltage dependence

$$J_S = J_{SO} \exp \left[.0956 \, (F)^{\frac{1}{2}}/T \right] \tag{21}$$

If log J vs. $(F)^{\frac{1}{2}}$ is plotted a straight line with a slope given by

$$.434 \left[\tfrac{1}{2}(e/\pi\epsilon)^{\frac{1}{2}}/kT\right] \tag{22}$$

results. For mks units this reduces to .0415/T. The experimental data are plotted in this fashion in Figures 14, 15, 16, and 17. It would appear, at first, that a Schottky emission behavior is evidenced, since the majority of the curves give a good straight line fit. The slopes of the experimental data do not agree with the values predicted by the Schottky model, however. The calculated values and observed

values are listed in Table IV for each of the test conditions. The value for the sample at 1350 Å and 117°K gives good agreement with the predicted value. All the other experimental values give significant deviations from predicted values. Examination of equation (22) shows that the dielectric constant is the only variable in the calculated slope not known to 1% accuracy or better and it would have to be in error by a factor of 2 or more to bring the calculated value and observed value into agreement. Therefore, the difference between the observed and the calculated slopes cannot be ascribed to errors in the calculated values. It is concluded that the Schottky model does not describe the observed data because of this lack of agreement between the calculated and predicted slope.

C. Fit of the Data to a Fowler-Nordheim Model

The Fowler-Nordheim model for tunnel emission predicts for following current-voltage behavior

$$\frac{J_F}{F^2} = B \exp (C/F) \tag{23}$$

For mks units B is given by

$$1.54 \times 10^{-10} / [\phi\, t^2(y)] \tag{24}$$

and C is given by

$$-6.83 \times 10^9\, \phi^{\frac{3}{2}}\, v(y). \tag{25}$$

A straight line with a slope given by equation (25) and an intercept given by equation (24) will result when log (J/F^2) is

plotted against 1/F. The experimental data are plotted in this fashion in Figures 18-23. If the data agreed with the model, the curves would be straight lines. But for each of the following conditions, the curves have either a positive slope, a definite curvature, or both:

1. At 380°K and 290°K for all specimens
2. At 215°K and 117°K for the 450 Å specimen
3. At all temperatures for the 1350 Å specimen

The analysis of the remaining nine tests is complicated because a value of Ø could not be found for the tantalum-tantalum oxide interface and therefore exact values for the slope cannot be calculated for comparison with the observed value.

A technique which will permit the comparison of the experimental data and the predictions of the model is to calculate Ø from the slope of the curve using equation (25) and then use this value of Ø to calculate the intercept using equation (24). This calculated value of the intercept can then be compared with the intercept observed by extrapolating the experimental data. Use of this technique requires a trial and error solution because the function v(y) in the slope is an elliptic function of Ø and an explicit solution for Ø cannot be derived.

Since tunneling is most likely to be important at low temperatures and in thin films, the 50 Å, 117°K test was selected as being the most likely to exhibit tunneling. The observed slope from Figure 20 is 1.78×10^9. The value of y for the first approximate calculation of Ø was determined by using an F of 225×10^6 volts/meter and the work

function of tantalum, 4.2 electron volts[16]. This value of Ø was selected as a starting point since the maximum value of Ø that could be expected was the work function of tantalum into a vacuum. The value of y calculated from these numbers was .132. Values v(y) were obtained from Good and Muller[10]. Successive approximations yielded a final value .993 ev for Ø when the slope was -1.78×10^9 and F was 225×10^6 volts/meter. Using this value of Ø in equation (24), and assuming t(y) was one (this assumption appears valid since t(y) ranges from 1.0 to 1.1[10]) yielded a value of 2.45×10^{-10} amp/volt^2. Thus, the model predicts that a specimen with a slope of 1.78×10^9 should have an intercept of 1.55×10^{-10} amp /volt^2. The actual intercept for this specimen was 2.7×10^{-15} amp /volt^2.

On this basis it is concluded that this sample under these test conditions does not fit the Fowler-Nordheim model. Since it is the most likely condition to fit the model, the Fowler-Nordheim model is rejected.

The model can also be rejected for these data by considering the intercepts alone. Examination of equation (24) shows the intercept will be a minimum when Ø and t(y) are maximum. Since the maximum value of Ø is the 4.2 ev work function of tantalum into a vacuum and of t(y) is 1.1[10], the minimum value of the intercept can be calculated to be 3.03×10^{-11} amp /volt^2. Examination of Figures 21, 22 and 23 shows this is several orders of magnitude larger than the intercept for the experimental data. The intercepts for these curves are shown in Table V.

D. Fit of the Data to Simultaneous Thermionic Emission and Tunneling

The possibility that simultaneous Schottky and Fowler-Nordheim emission was occurring was next considered. Murphy and Good[17] develop a general equation for emission at a metal-insulator interface. They show that this general relation can be reduced to the Schottky relation or to the Fowler-Nordheim relation if the field and temperature fall between certain limits. The region where the general equation reduces to the Schottky case is defined in terms of a parameter

$$P = (F)^{\frac{3}{4}} / kT \qquad (26)$$

The field and energy in this expression are expressed in dimensionless Hartree units. These are obtained by dividing field by $16\pi^4 m^2 e^5/h^4 = 5.15 \times 10^{11}$ volts/meter and dividing energy by $4\pi^2 me^4/h^2 = 27.2$ ev. Their development requires that P be less than 1. For the conditions of this experiment this condition was not met, so that it was not possible to fit the data to the combined emission expression.

E. Fit of the Data to Mead's Model

Mead's proposals for the conduction mechanism were:

1. Tunneling across the metal-oxide interface at low temperature and low field.
2. Ohmic conduction at high temperature and low field due to electrons jumping from one trap site to the next.
3. Field ionization of traps at low temperatures and high fields.
4. Thermal excitation of traps at high temperatures and high fields.

Each of these four proposals was considered in turn to determine if the experimental data would satisfy such a model. The tunneling proposed in the first point is described by the Fowler-Nordheim model and it was demonstrated in section IV-C that the data did not fit a Fowler-Nordheim plot. Therefore, this effect is not present.

The ohmic behavior of the second point is present.

Field ionization of traps as given by equation (17) has the same mathematical form as the Fowler-Nordheim equation (4). It was demonstrated in section IV-C of this thesis that the data did not fit the Fowler-Nordheim equation, so it is concluded that the mechanism of field ionization of traps is not occurring.

The fourth proposal of thermal excitation of traps is described by the equation

$$J = CF \exp - \left\{ e\left[\psi - (eF/\pi \epsilon)^{\frac{1}{2}} \right] / kT \right\} \qquad (29)$$

If log J/F vs. $(F)^{\frac{1}{2}}$ is plotted, a straight line should result. This is done in Figure 24. It is obvious the curves are not straight lines. So this effect is not present.

It has been shown that only one of the four effects predicted by Mead's theory is evidenced by the data. Therefore, it is concluded that these data do not fit Mead's theory.

F. Summary

Four possible mechanisms for electronic conduction in tantalum pentoxide anodically formed on beta tantalum were considered. These were:

1. Space charge limiting of current as suggested by Lampert[6].
2. Field enhanced, thermionic emission as described by the Schottky equation (8).
3. Tunneling as described by the Fowler-Nordheim equation[10].
4. Trap excitation by several mechanisms as described by Mead[5].

It was concluded that the data best fit the predictions of the space charge limiting theories.

V. SUGGESTIONS FOR FURTHER WORK

There were three effects noted during the experimental part of the work which could be investigated further. These were an anomalous capacitance effect, a time-dependent voltage-current relation, and an irreversible change in the conductivity of the oxide.

Anomalous Capacitance Effect

One of the techniques used to measure the thickness of films is by capacitance measurements. In this technique the film is used as the dielectric of a parallel plate capacitor and the thickness calculated from the formula

$$C = \epsilon A/d \qquad (30)$$

C = capacitance

A = Area

other symbols as previously defined. When the capacitance of the specimens in this experiment were measured it was found that they differed from the predicted values by several orders of magnitude. The predicted values are based upon the thickness calculated from the anodization constant. Table VI lists predicted and observed values for several specimens. If 1/C is plotted against d as in Figure 25, the intercept at d = 0 is not at 0 but at some finite value. The behavior suggests that a capacitance of the order of 5000 uuf is in series with the oxide structure. A similar effect was reported by Mead[18]. This may also account for the high anodization constant reported by Namba, et al.[19], since they de-

termined the anodization constant by capacitance measurements on films.

Relaxation Effects

It was observed, when the ramp voltage was applied to the thicker specimens at lower temperatures, that the current would decrease at first. Several specimens were tested by applying a DC voltage and the same effect was observed. Maissel and Standley[4] and others have reported similar effects. Since the temperatures are such that ionic conduction can be neglected and the voltage is continuously increasing, it would appear that this effect might be due to a relaxation time associated with the filling of the trap sites.

Irreversible Conductivity Change

It was observed that if the voltage applied to the specimen exceeded a certain value the current-voltage characteristic changed irreversibly. The magnitude of the voltage varied with the thickness but was not directly dependent upon it, i.e., thicker films would tolerate higher voltages but not in a linear fashion.

The effect was studied only to establish safe voltages for measurements. The change did not affect the conductivity mechanism. Behavior for a particular specimen once it had changed obeyed the same relationship as prior to the change but, because differences between successive tests could not completely be ascribed to the independent parameters it was necessary to restrict the range of voltages covered.

It is suggested that all three of these effects are suitable subjects for further study by those interested in conduction mechanisms in oxides.

TABLE I

Tantalum Thicknesses as Deposited

Slide Number	Talysurf Measurement	Beta Backscatter
M-5009	5797 A	6070 A
M-5010	5857 A	6080 A
M-5171	5905 A	6030 A
M-5172	5989 A	6010 A
M-5173	5995 A	6180 A

TABLE II

Maximum Values of Test Voltages

Temp.	d				
°K	50 A	150 A	450 A	1350 A	4050 A
380	.10V	.35V	1.0V	2.5V	2.5V
290	.85V	.85V	2.5V	6.0V	7.5V
215	1.20V	1.25V	3.0V	7.5V	9.0V
148	1.25V	1.50V	4.5V	8.0V	9.5V
117	1.40V	1.75V	5.5V	8.5V	10.0V
100	1.75V	2.00V	6.0V	9.0V	10.5V

TABLE III

Experimental and Calculated Data

d $\overset{o}{A}$	T ^{o}K	I uua	V Volts	J A/M^2 $\times 10^{-6}$	F Volts/M $\times 10^{6}$	$(F)^{\frac{1}{2}}$ $(Volts/M)^{\frac{1}{2}}$ $\times 10^{3}$	J/F^2 Amp/V^2 $\times 10^{-20}$	1/F M/Volt $\times 10^{-8}$
50	382	6.5	.02	4.92	4.00	2.00	30.750	25.000
50	382	11.0	.04	8.33	8.00	2.83	13.016	12.500
50	382	14.0	.06	10.60	12.00	3.46	7.361	8.330
50	382	18.5	.08	14.00	16.00	4.00	5.469	6.250
50	382	22.0	.10	16.65	20.00	4.47	4.163	5.000
50	290	3.0	.20	2.27	40.00	6.32	.142	2.500
50	290	6.0	.40	4.54	80.00	8.94	.071	1.250
50	290	10.5	.60	7.95	120.00	10.95	.055	.833
50	290	16.2	.72	12.26	144.00	12.00	.059	.694
50	290	27.0	.80	20.44	160.00	12.65	.080	.625
50	215	0	.72	0	144.00	12.00	0	.694
50	215	3.0	.80	2.27	160.00	12.65	.009	.625
50	215	7.5	.88	5.68	176.00	13.27	.018	.568
50	215	15.0	.92	11.36	184.00	13.56	.034	.543
50	215	79.0	1.00	59.80	200.00	14.14	.149	.500
50	148	0	.83	0	166.00	12.88	0	.602
50	148	18.0	.96	13.63	192.00	13.85	.037	.521
50	148	97.5	1.05	73.81	210.00	14.49	.167	.476
50	148	127.5	1.09	96.52	218.00	14.76	.203	.459
50	117	0	.85	0	166.00	12.88	0	.602
50	117	4.6	1.08	3.48	216.00	14.70	.007	.463
50	117	40.5	1.20	30.65	240.00	15.49	.053	.417
50	117	121.5	1.28	91.98	256.00	16.00	.140	.391

TABLE III (Cont.)

d o A	T ^{o}K	I uua	V Volts	J A/M^2 $x10^{-6}$	F Volts/M $x10^{6}$	$(F)^{\frac{1}{2}}$ $(Volts/M)^{\frac{1}{2}}$ $x10^{3}$	J/F^2 Amp/V^2 $x10^{-20}$	1/F M/Volt $x10^{-8}$
150	381	15.0	.02	11.36	1.33	1.15	642.400	75.188
150	381	28.0	.05	21.20	3.34	1.83	190.040	29.940
150	381	45.0	.12	34.07	8.00	2.83	53.230	12.500
150	381	70.0	.19	53.37	12.67	3.56	33.240	7.893
150	381	85.3	.24	64.57	16.01	4.00	25.190	6.246
150	381	103.5	.29	78.35	19.34	4.40	20.950	5.171
150	290	7.2	.20	5.45	13.34	3.65	3.063	7.496
150	290	13.2	.40	9.99	26.68	5.17	1.391	3.748
150	290	25.8	.60	19.53	40.02	6.33	1.210	2.499
150	290	46.3	.72	35.05	48.02	6.93	1.520	2.082
150	215	5.0	.68	3.79	45.36	6.73	.184	2.205
150	215	26.3	.88	19.91	58.70	7.66	.578	1.704
150	215	48.0	1.00	36.34	66.70	8.17	.817	1.499
150	147	6.0	.72	4.54	48.02	6.93	.197	2.082
150	147	21.0	.96	15.90	64.03	8.00	.388	1.562
150	147	78.0	1.20	59.05	80.04	8.95	.922	1.249
150	147	141.0	1.32	106.74	88.04	9.38	1.377	1.136
150	117	7.5	1.20	5.68	80.04	8.95	.089	1.249
150	117	28.5	1.32	21.57	88.04	9.38	.278	1.136
150	117	60.0	1.44	45.42	96.05	9.80	.492	1.104
150	117	127.5	1.57	96.52	104.72	10.23	.880	.955

TABLE III (Cont.)

d $\overset{o}{A}$	T ^{o}K	I uua	V Volts	J A/M^2 $\times 10^{-6}$	F (Volts/M $\times 10^{6}$	$(F)^{\frac{1}{2}}$ $(Volts/M)^{\frac{1}{2}}$ $\times 10^{3}$	J/F^2 Amp/V^2 $\times 10^{-20}$	1/F M/Volt $\times 10^{-8}$
150	105	4.5	.96	3.41	64.03	8.00	.083	1.562
150	105	9.0	1.08	6.81	72.04	8.49	.131	1.388
150	105	22.5	1.20	17.03	80.04	8.95	.266	1.249
150	105	55.0	1.32	41.64	88.04	9.38	.537	1.136
450	381	15.0	.07	11.36	1.55	1.24	472.841	64.516
450	381	20.5	.20	15.52	4.44	2.11	78.727	22.523
450	381	36.0	.40	27.25	8.88	2.98	34.557	11.261
450	381	60.0	.60	45.42	13.32	3.65	25.600	7.508
450	381	83.0	.80	62.83	17.76	4.21	19.920	5.631
450	290	4.0	.84	3.03	18.65	4.32	.871	5.362
450	290	9.0	1.32	6.81	29.30	5.41	.793	3.413
450	290	22.0	1.80	16.65	39.96	6.32	1.062	2.503
450	290	57.0	2.24	43.15	49.73	7.05	1.745	2.011
450	214	0	1.20	0	26.64	5.16	0	3.754
450	214	5.0	1.80	3.78	39.96	6.32	.237	2.503
450	214	15.0	2.24	11.36	49.73	7.05	.459	2.011
450	214	29.0	2.75	21.95	61.05	7.81	.589	1.638
450	148	0	2.80	0	62.16	7.88	0	1.609
450	148	10.0	4.00	7.57	88.80	9.42	.096	1.126
450	148	40.0	4.80	30.28	106.56	10.32	.267	.938
450	148	130.0	5.60	98.41	124.32	11.15	.637	.804
450	148	190.0	6.00	143.83	133.20	11.54	.811	.751

TABLE III (Cont.)

d o A	T °K	I uua	V Volts	J A/M^2 $x10^{-6}$	F Volts/M $x10^6$	$(F)^{\frac{1}{2}}$ $(Volts/M)^{\frac{1}{2}}$ $x10^3$	J/F^2 Amp/V^2 $x10^{-20}$	1/F M/Volt $x10^{-8}$
450	114	0	2.00	0	44.40	6.66	0	2.252
450	114	46.0	4.00	34.82	88.80	9.42	.442	1.126
450	114	80.0	5.60	60.56	124.32	11.15	.392	.804
450	114	90.0	6.40	68.13	142.08	11.92	.337	.704
450	114	96.0	7.20	72.67	159.84	12.64	.284	.626
450	101	0	2.00	0	44.40	6.66	0	2.252
450	101	3.0	2.40	2.27	53.28	7.30	.080	1.887
450	101	13.5	3.20	10.22	71.04	8.43	.203	1.408
450	101	33.0	4.00	24.98	88.80	9.42	.317	1.126
450	101	56.0	4.80	42.39	106.56	10.32	.373	.938
450	101	72.0	5.60	54.50	124.32	11.15	.353	.804
450	101	85.0	6.40	64.34	142.08	11.92	.319	.704
1350	380	9.0	.48	6.81	3.55	1.88	54.037	28.169
1350	380	18.0	.96	13.63	7.10	2.66	27.038	14.085
1350	380	27.0	1.44	20.44	10.66	3.26	17.987	9.381
1350	380	33.0	1.92	24.98	14.21	3.77	12.371	7.037
1350	290	1.5	2.00	1.14	14.80	3.85	.520	6.757
1350	290	6.8	3.00	5.15	22.20	4.71	1.045	4.505
1350	290	13.5	4.00	10.22	29.60	5.44	1.166	3.378
1350	290	31.5	6.00	23.85	44.40	6.66	1.210	2.252
1350	214	4.5	4.00	3.41	29.60	5.44	.389	3.378
1350	214	18.3	5.60	13.85	41.44	6.55	.807	2.413
1350	214	24.5	6.80	18.55	50.32	7.09	.733	1.987

TABLE III (Cont.)

d o A	T ^{o}K	I uua	V Volts	J A/M^2 $x10^{-6}$	F Volts/M $x10^{6}$	$(F)^{\frac{1}{2}}$ $(Volts/M)^{\frac{1}{2}}$ $x10^{3}$	J/F^2 Amp/V^2 $x10^{-20}$	1/F M/Volt $x10^{-8}$
1350	147	1.5	6.40	1.14	47.36	6.88	.051	2.111
1350	147	6.0	8.00	4.54	59.20	7.69	.130	1.689
1350	147	8.0	9.20	6.06	68.08	8.25	.131	1.469
1350	117	3.0	5.60	2.27	41.44	6.44	.132	2.413
1350	117	4.5	6.40	3.41	47.36	6.88	.152	2.111
1350	117	6.5	8.00	4.92	59.20	7.69	.140	1.689
1350	117	7.0	8.80	5.30	65.12	8.07	.125	1.536
1350	117	7.5	10.00	5.68	74.00	8.60	.104	1.351
1350	97	1.0	5.60	.76	37.00	6.08	.055	2.703
1350	97	2.0	5.60	1.52	41.44	6.44	.088	2.413
1350	97	3.0	6.40	2.28	47.36	6.88	.102	2.111
1350	97	4.5	7.60	3.41	56.24	7.50	.109	1.778

TABLE IV

Slopes of Schottky Plots

T °K	Calculated Slope $(10^{-6}m/v)^{\frac{1}{2}}$	Observed Slope 50 A $(10^{-6}m/v)^{\frac{1}{2}}$	150 A $(10^{-6}m/v)^{\frac{1}{2}}$	450 A $(10^{-6}m/v)^{\frac{1}{2}}$	1350 A $(10^{-6}m/v)^{\frac{1}{2}}$
382	.109	.218	.301	.279	.398
290	.143	.342	.322	.477	.763
215	.193	1.130	.602	.505	.623
148	.280	1.130	.653	.653	.740
117	.354	1.060	.813	B	.398
100	.415	A	.903	.544	.301

A - No observation

B - Not calculated

TABLE V

Intercepts from Fowler-Nordheim Plots

Calculated Intercept (ϕ = 4.2 ev) = 3.03×10^{-11} amp/v^2

d A	T ^{o}K	Intercept Amp/Volt^2
50	215	7.0×10^{-15}
50	149	3.7×10^{-16}
50	117	2.7×10^{-14}
150	215	2.0×10^{-19}
150	147	3.8×10^{-19}
150	117	1.5×10^{-17}
150	100	3.6×10^{-18}
450	148	7.2×10^{-19}

TABLE VI

Observed and Calculated Capacitance for Samples

Specimen No.	d	Calculated Capacitance	Observed Capacitance		
			M-5009	M-5010	M-5174
	A	uuf	uuf	uuf	uuf
A1	50	49,200	A	A	6432
A2	50	49,200	A	A	6978
A3	50	49,200	A	6820	6329
A4	50	49,200	B	7481	6848
A5	50	49,200	A	A	4699
A6	50	49,200	4392	6044	4552
A7	50	49,200	4382	5680	4334
A8	50	49,200	B	6412	4608
B1	150	16,400	4027	4229	5931
B2	150	16,400	4318	6426	5982
B3	150	16,400	4244	6436	5848
B4	150	16,400	4186	4487	3751
B5	150	16,400	A	5213	3612
B6	150	16,400	4135	B	3624
B7	450	5,460	3276	4568	4236
B8	450	5,460	3272	4531	4234
B9	450	5,460	3378	3528	4188
B10	450	5,460	3001	3583	2831
B11	450	5,460	2836	3345	2700
B12	450	5,460	2918	3497	2695
C1	1350	1,820	1795	2283	C
C2	1350	1,820	1732	2004	2209
C3	1350	1,820	1821	B	C
C4	1350	1,820	1578	1660	1999
C5	1350	1,820	1540	1684	1543
C6	1350	1,820	1578	B	1524
C7	4050	607	761	972	908
C8	4050	607	831	971	C
C9	4050	607	905	1022	950
C10	4050	607	713	731	C
C11	4050	607	669	701	C
C12	4050	607	707	760	C

A - Specimen shorted
B - Overlapped adjacent thicker oxide
C - No connection between counter-electrode and tab

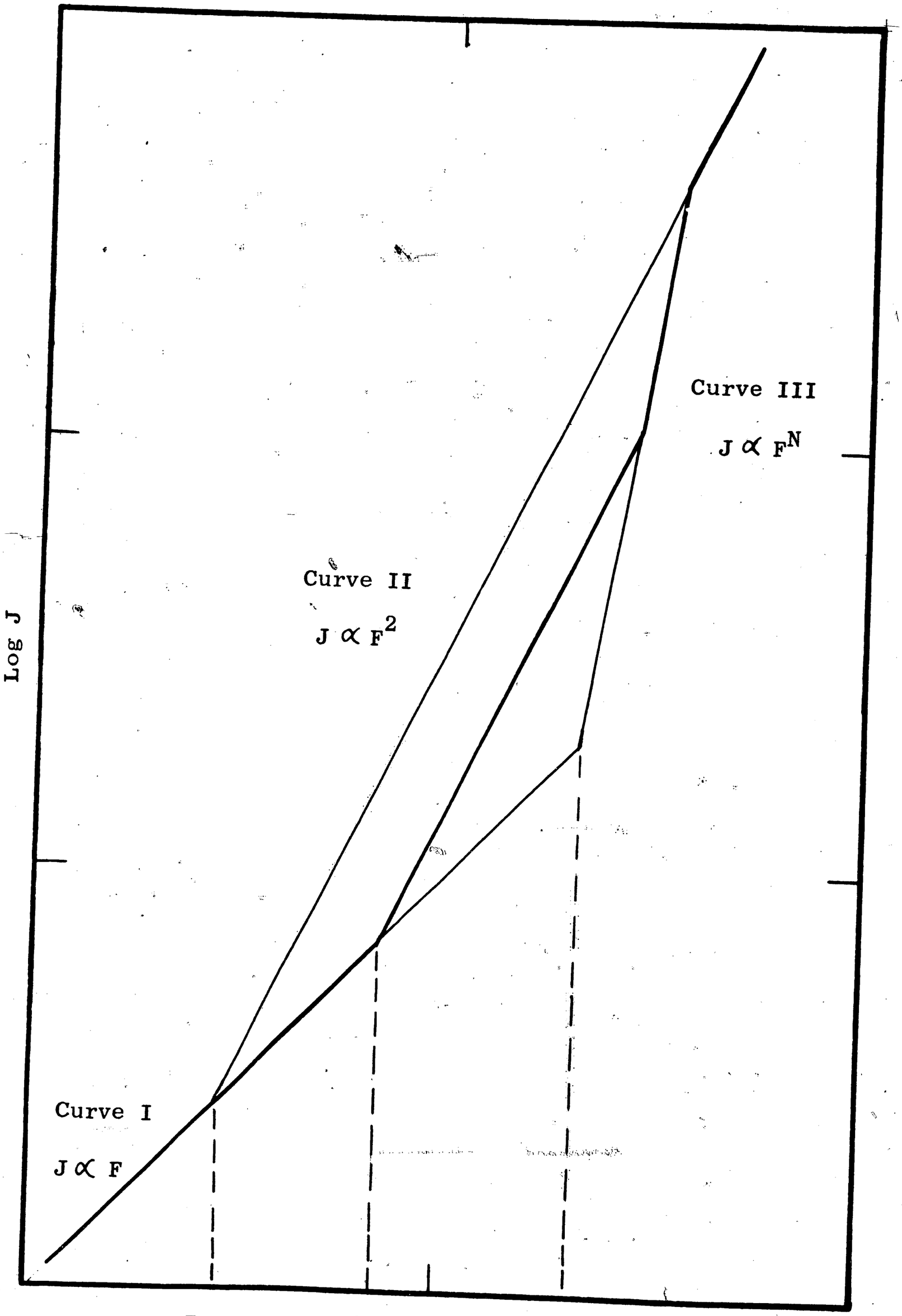

Figure 1. The Space Charge Limited Triangle

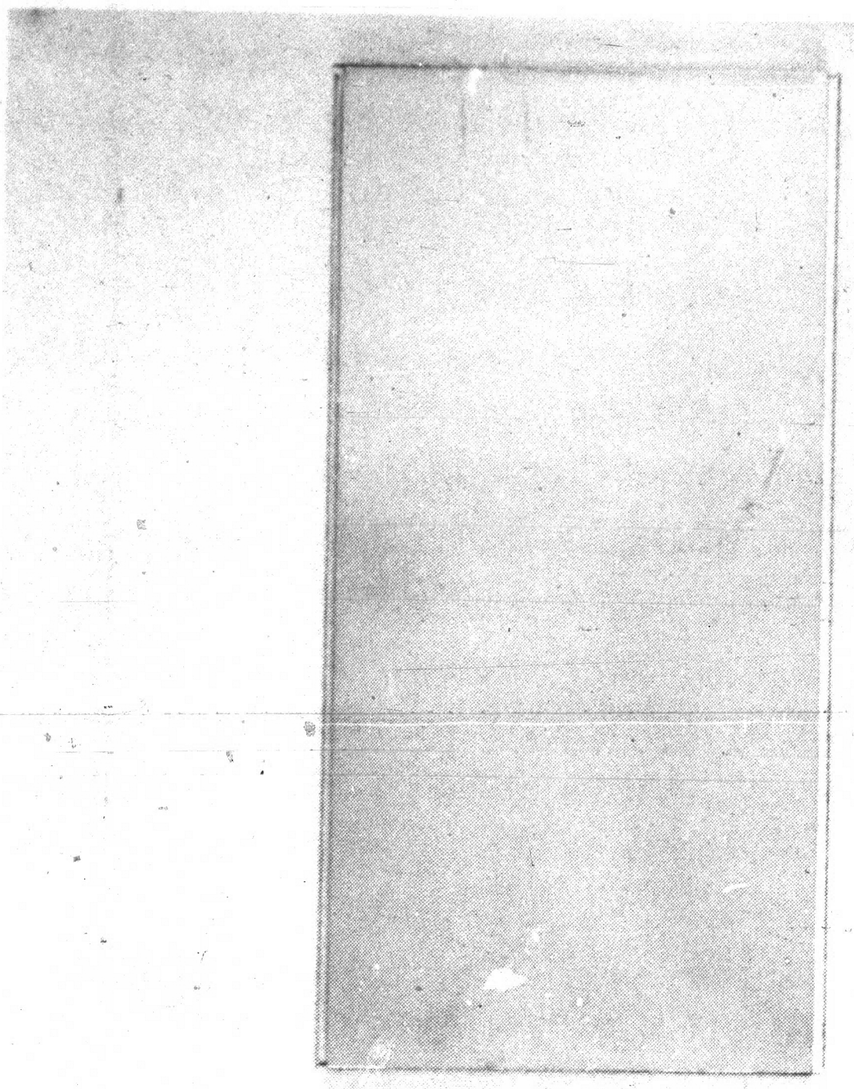

A. As sputtered

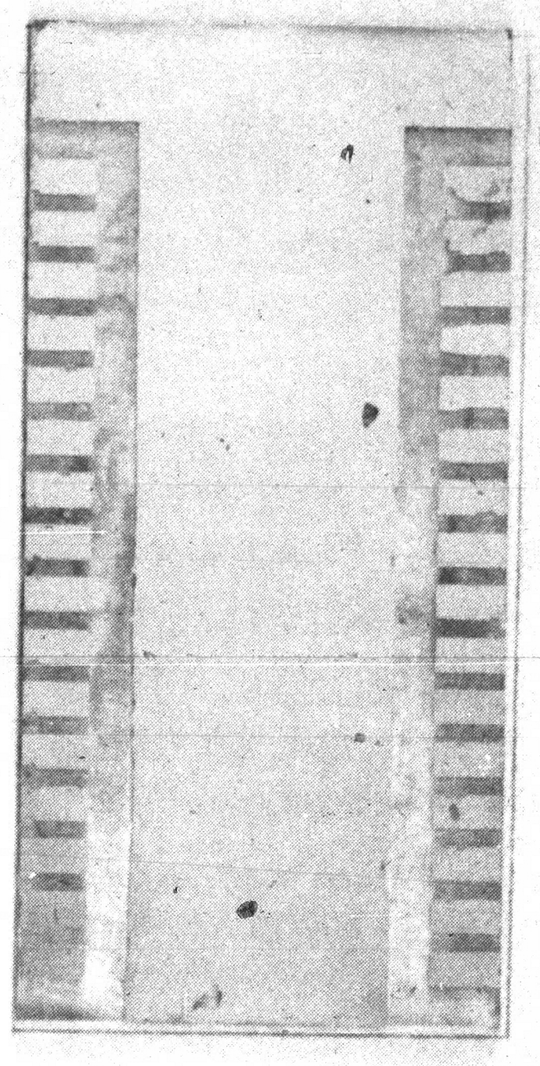

B. Etched

C. Anodized

D. Counter
Electrode Evaporated

Fig. 2. Experimental specimen in various stages of preparation.

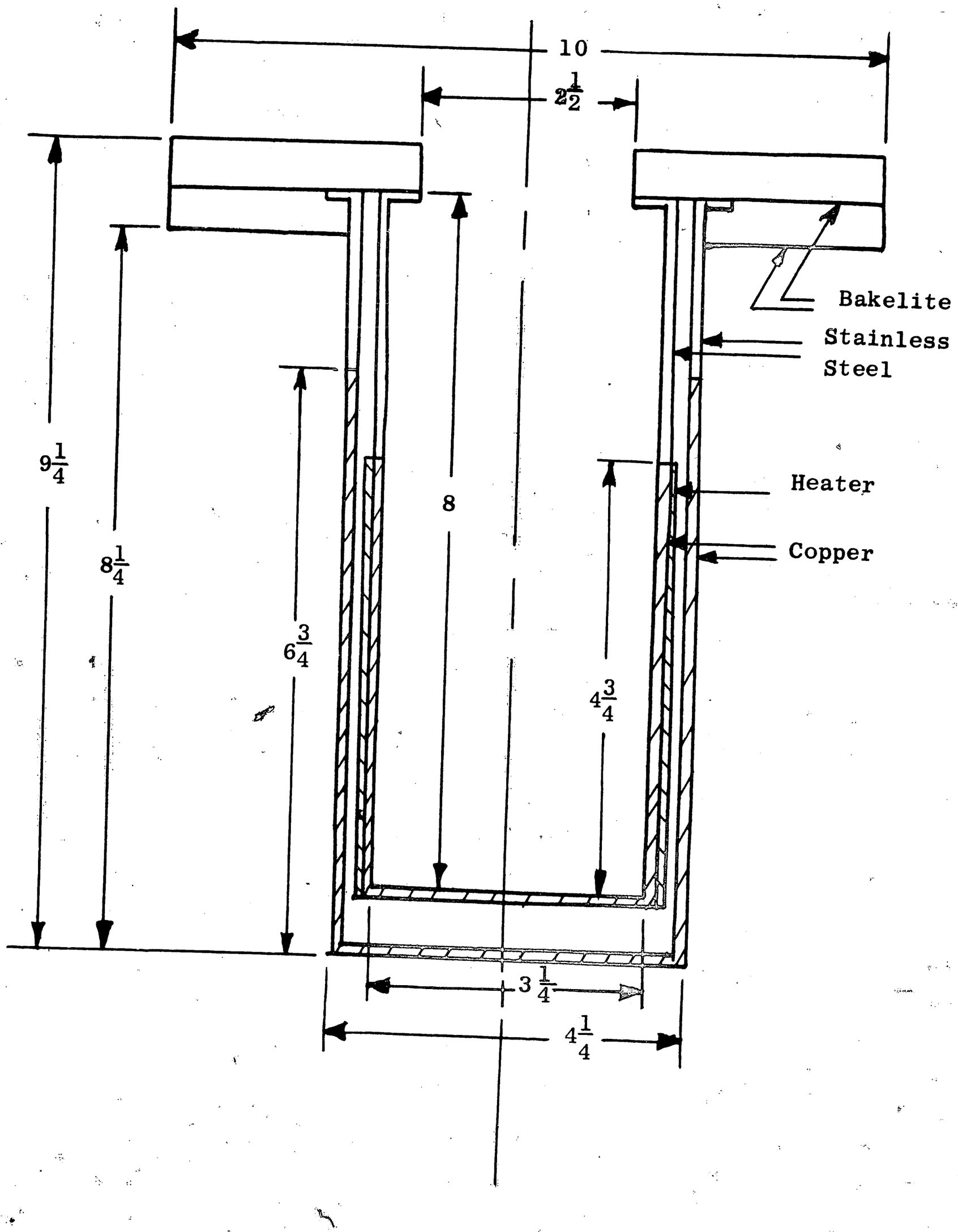

Figure 3. Cross Section of Environmental Chamber

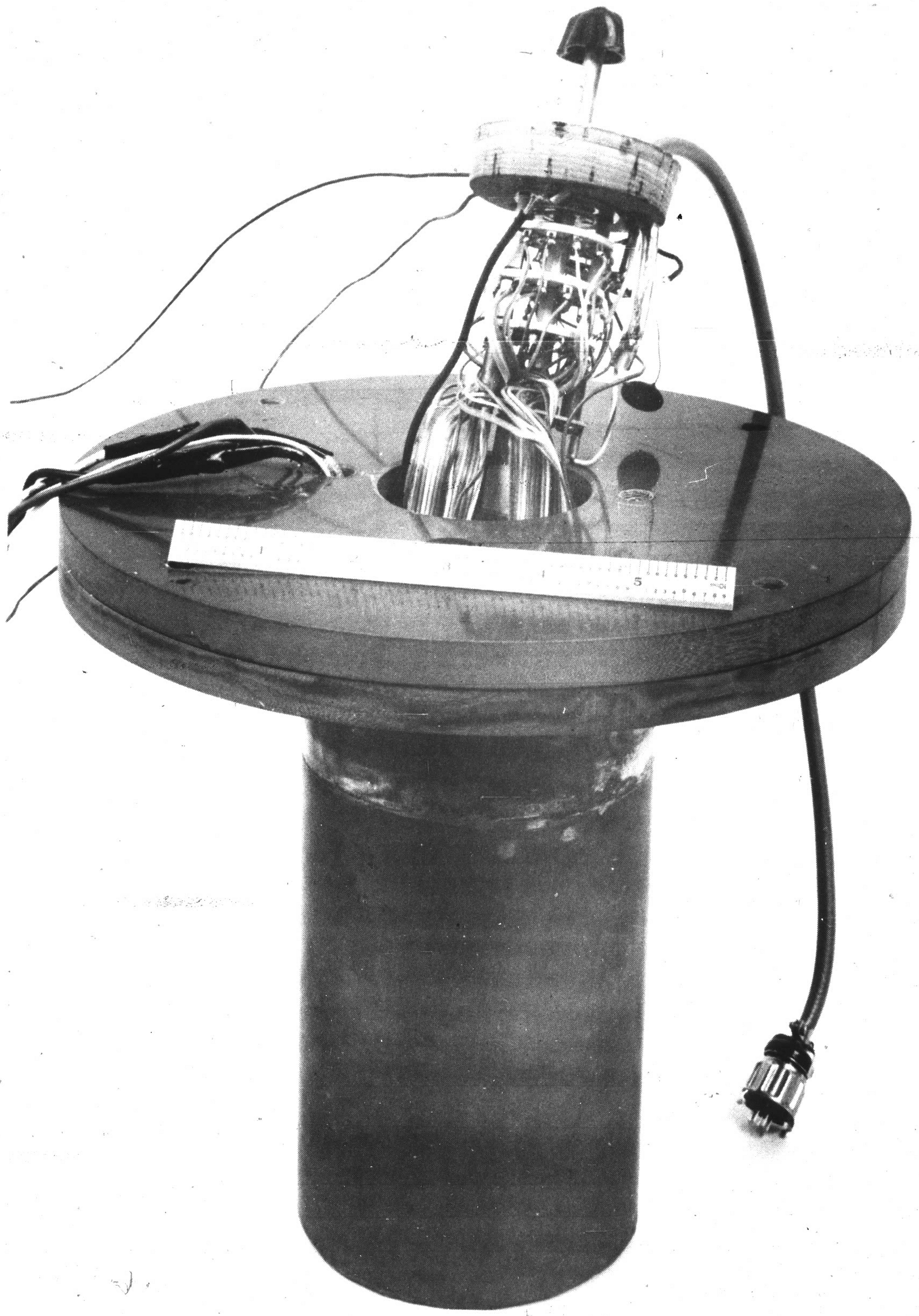

Figure 4. Environmental Equipment

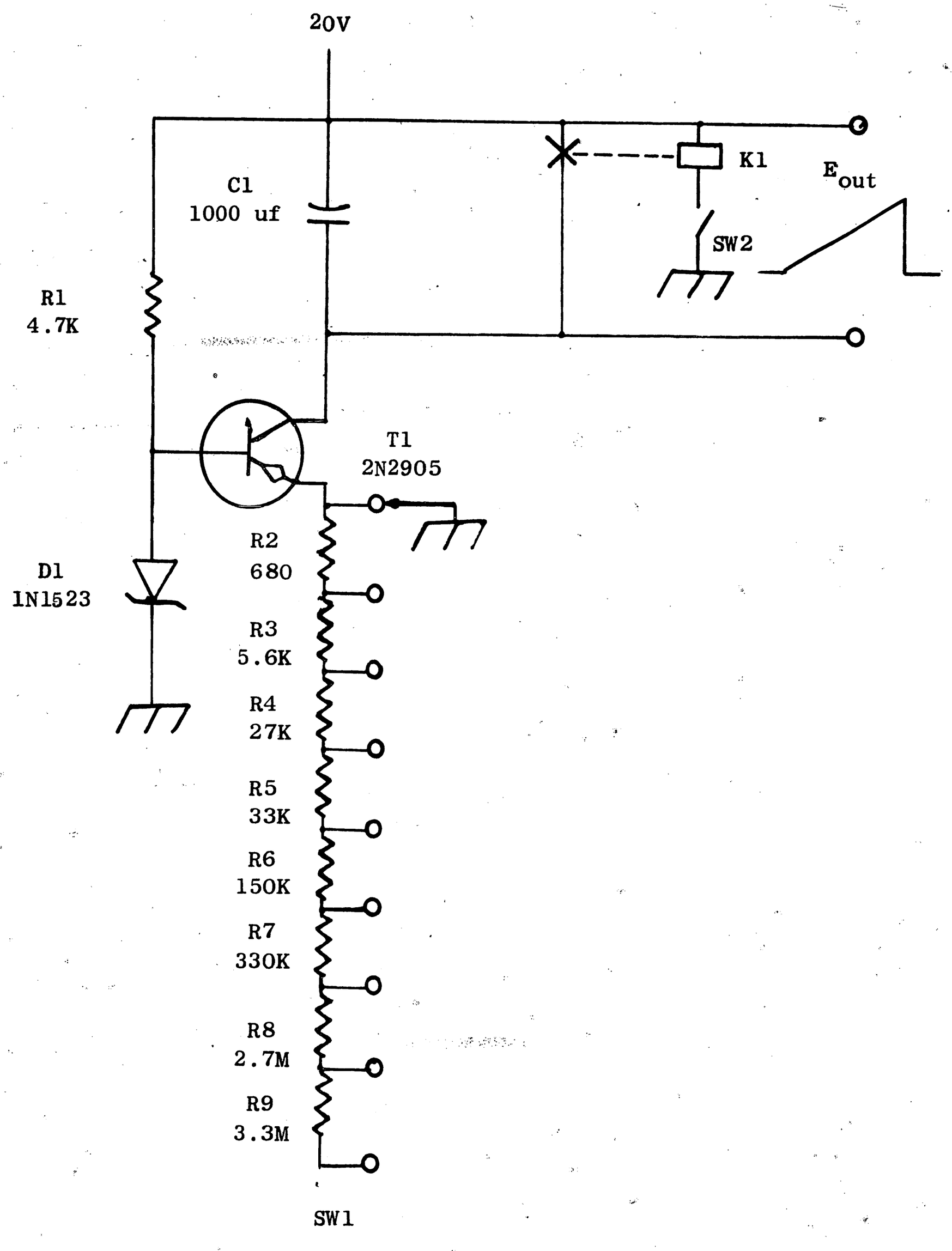

Figure 5. Ramp Generator Schematic

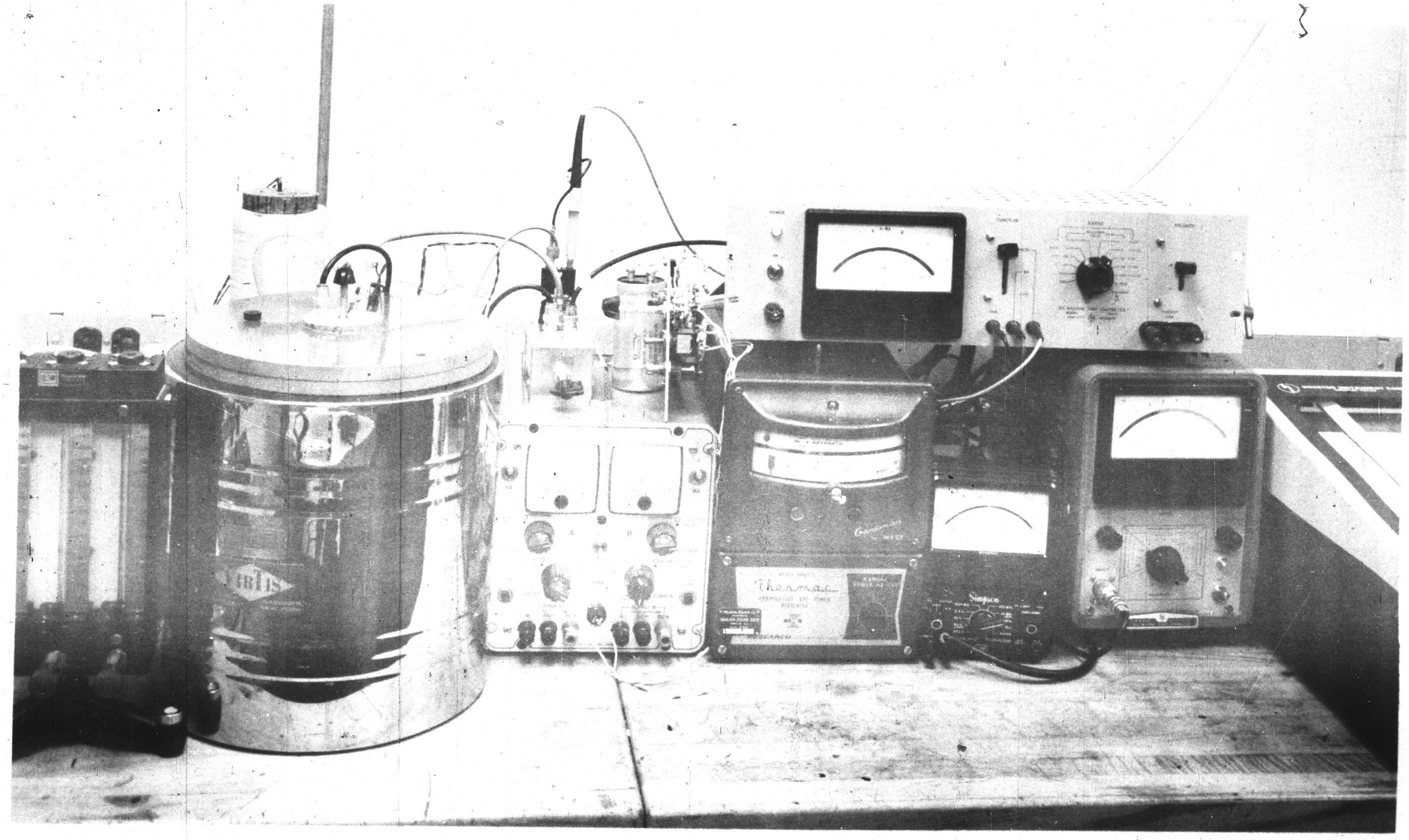

Figure 6. Experimental Equipment

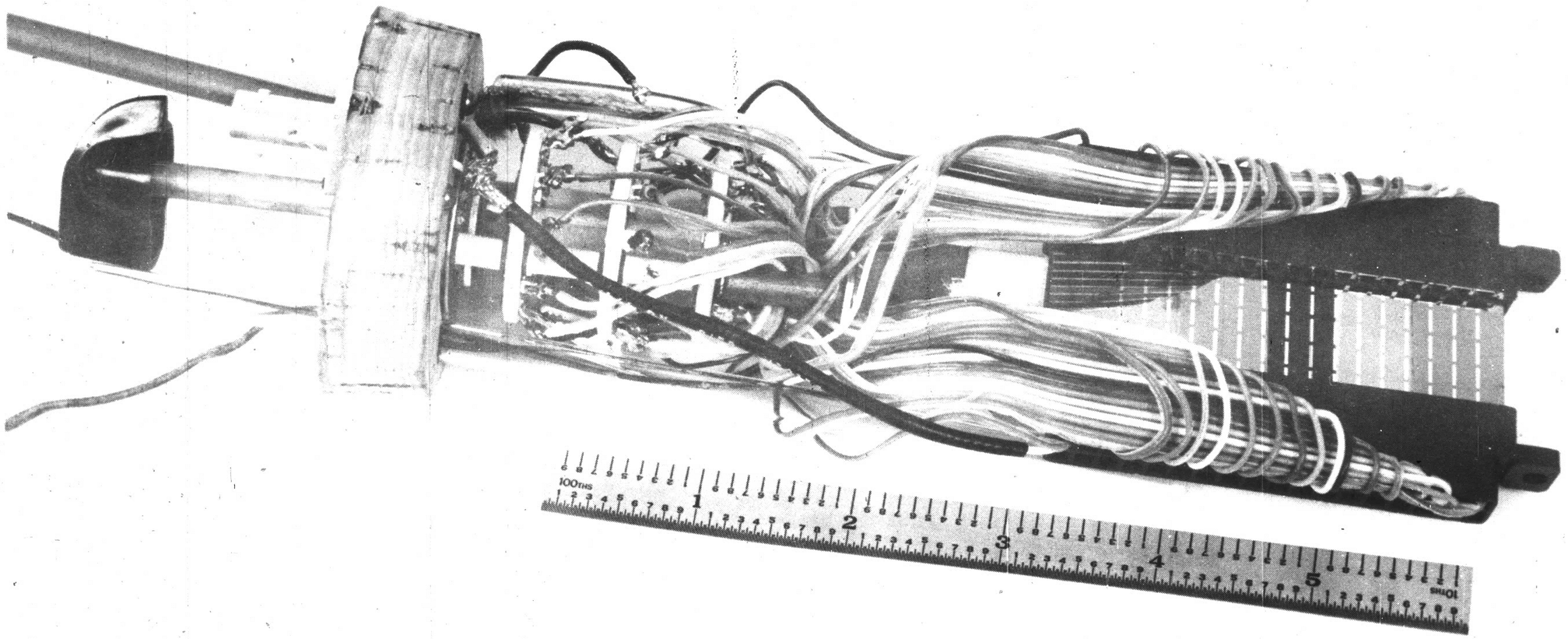

Figure 7. Holding Fixture

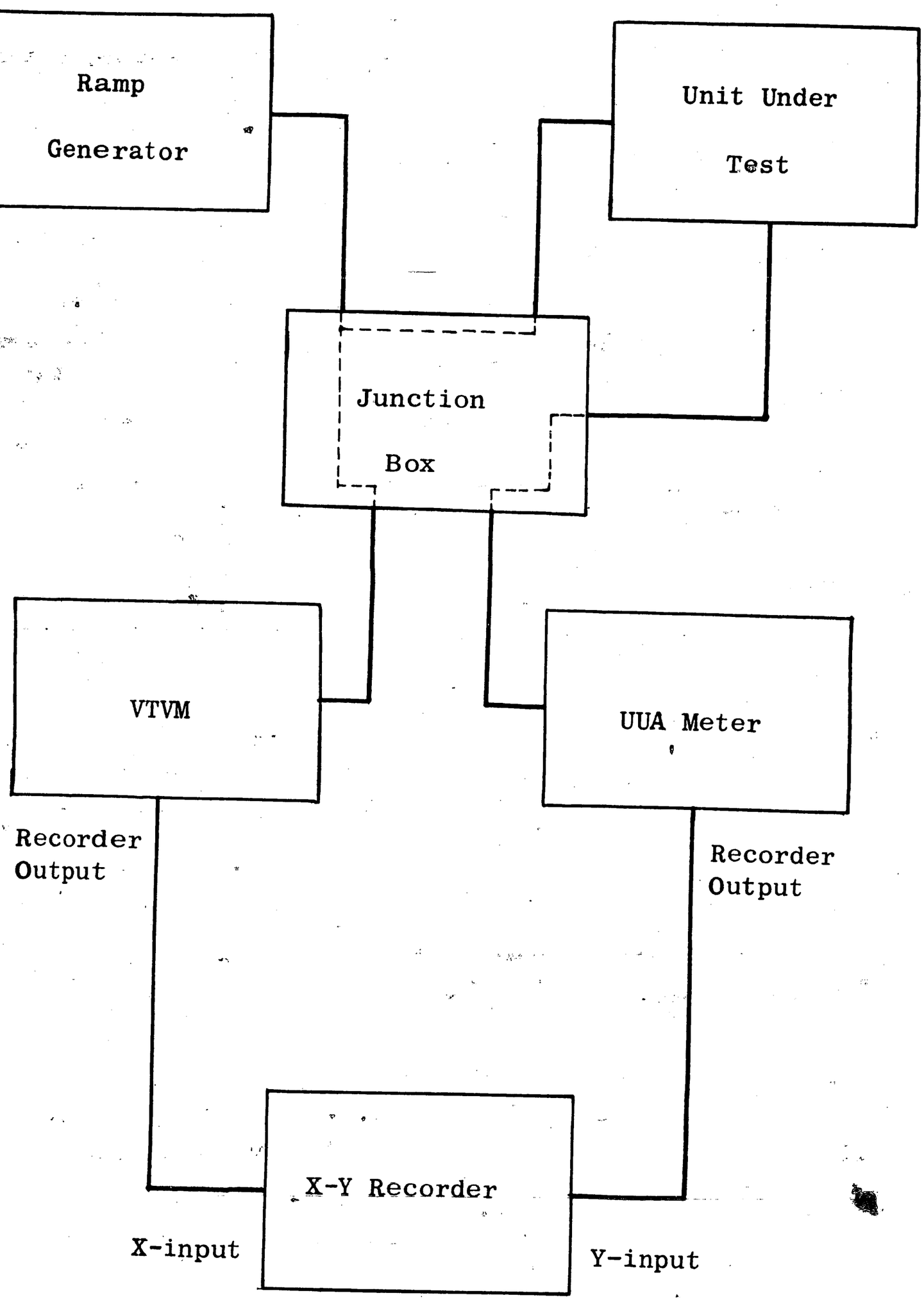

Figure 8. Block Diagram of Test Equipment

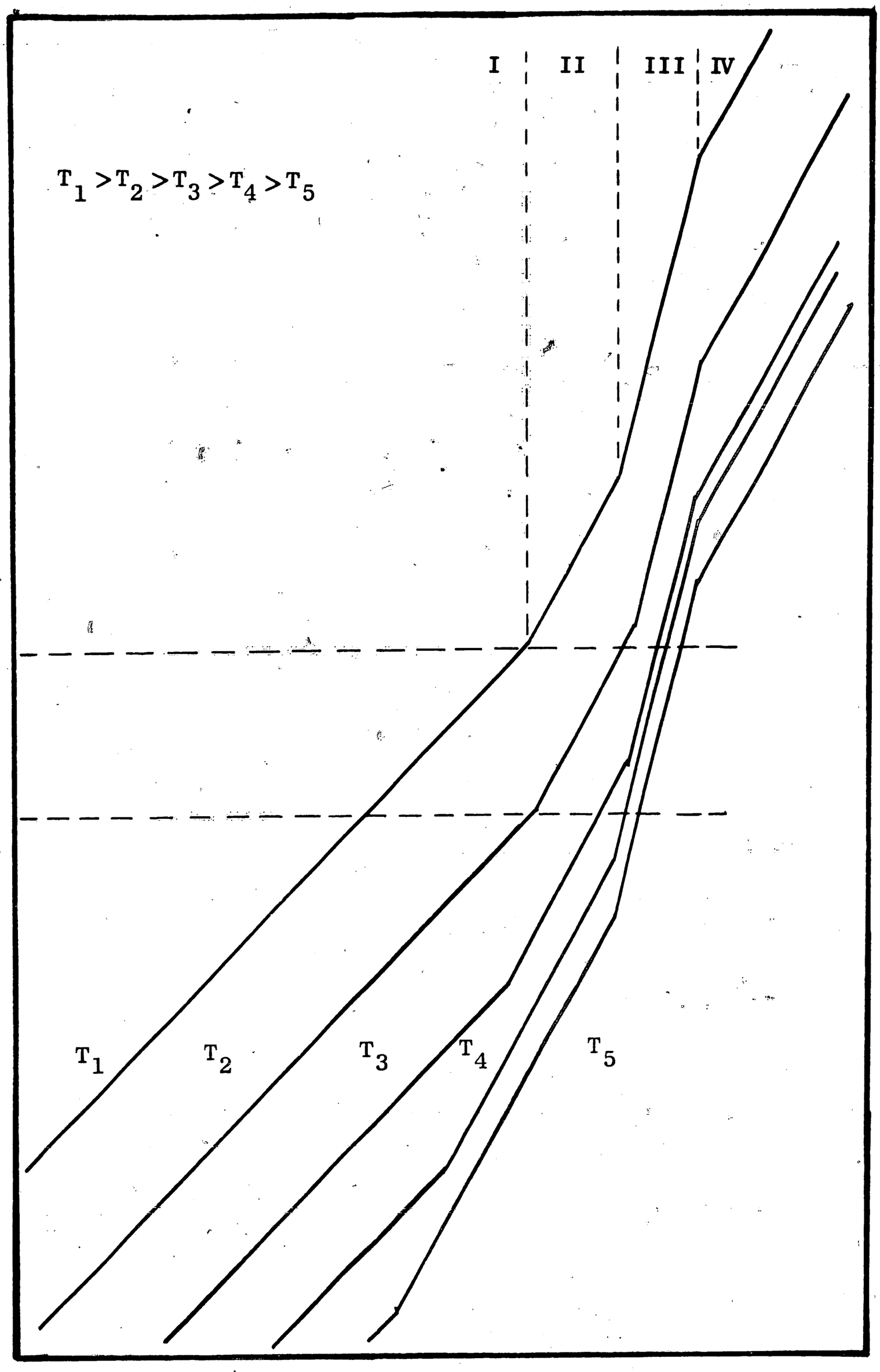

Figure 9. Effect of Temperature on SCL Characteristic Curve

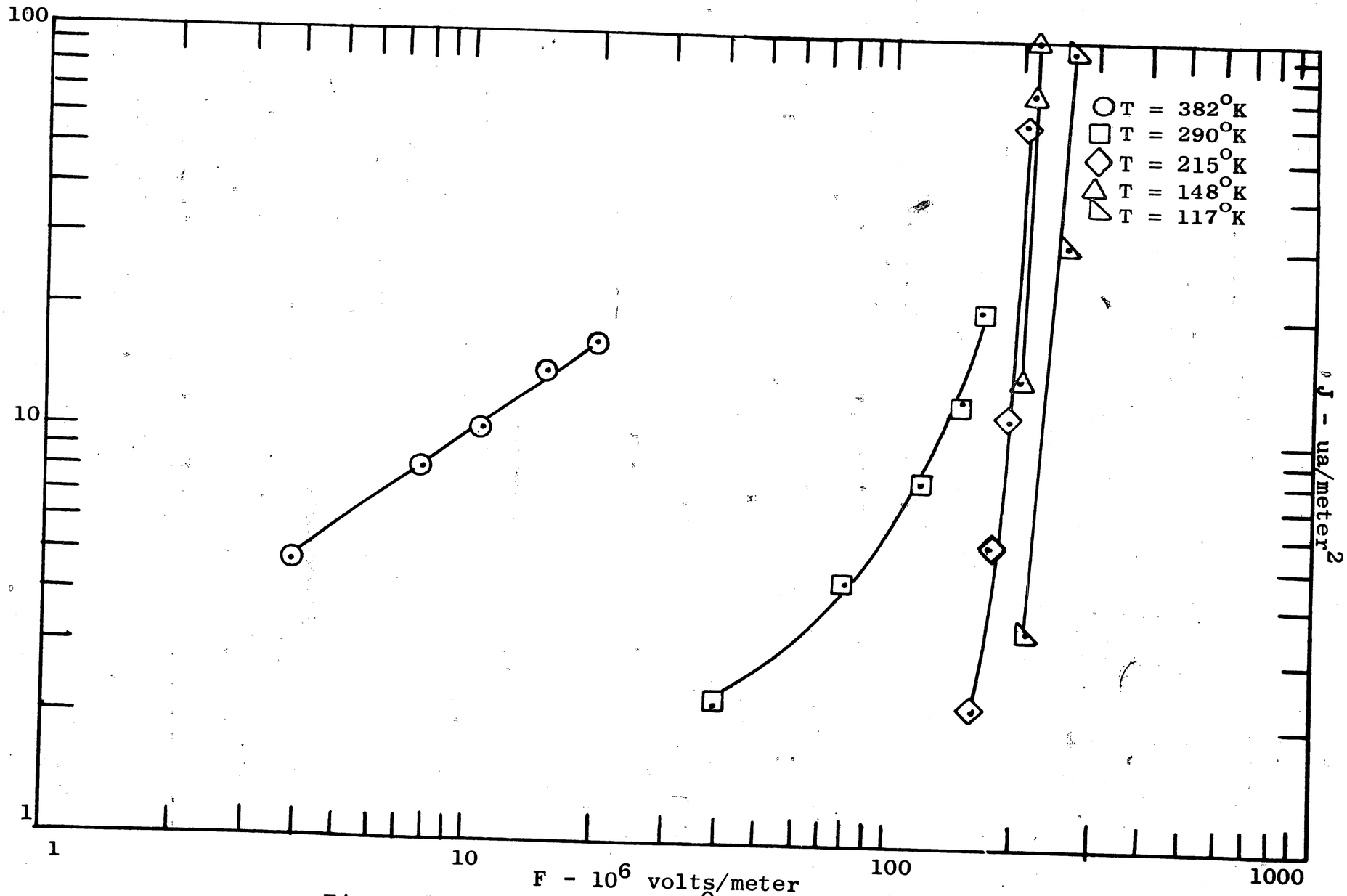

Figure 10. J vs. F for 50 Å

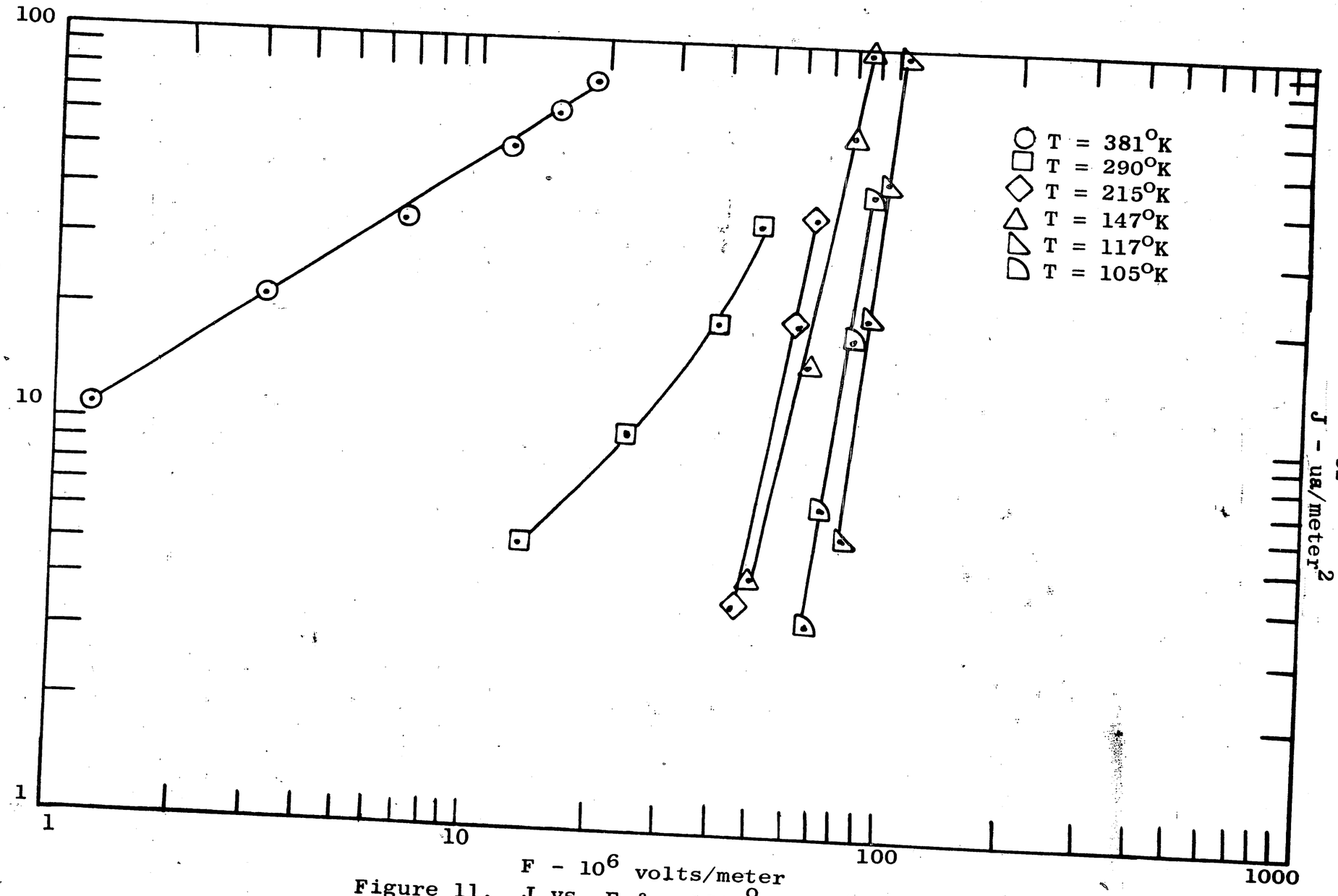

Figure 11. J vs. F for 150 Å

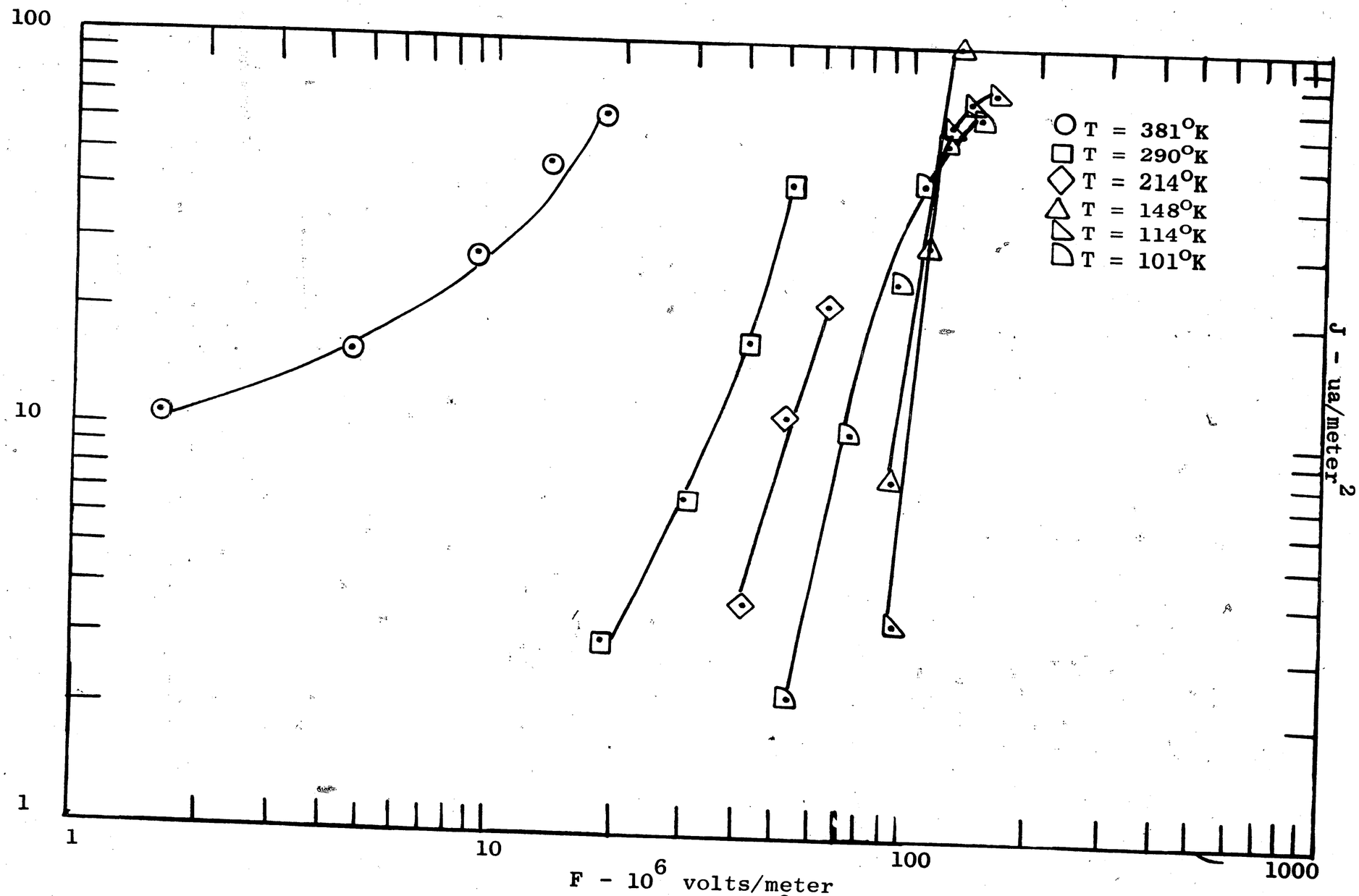

Figure 12. J vs. F for 450 Å

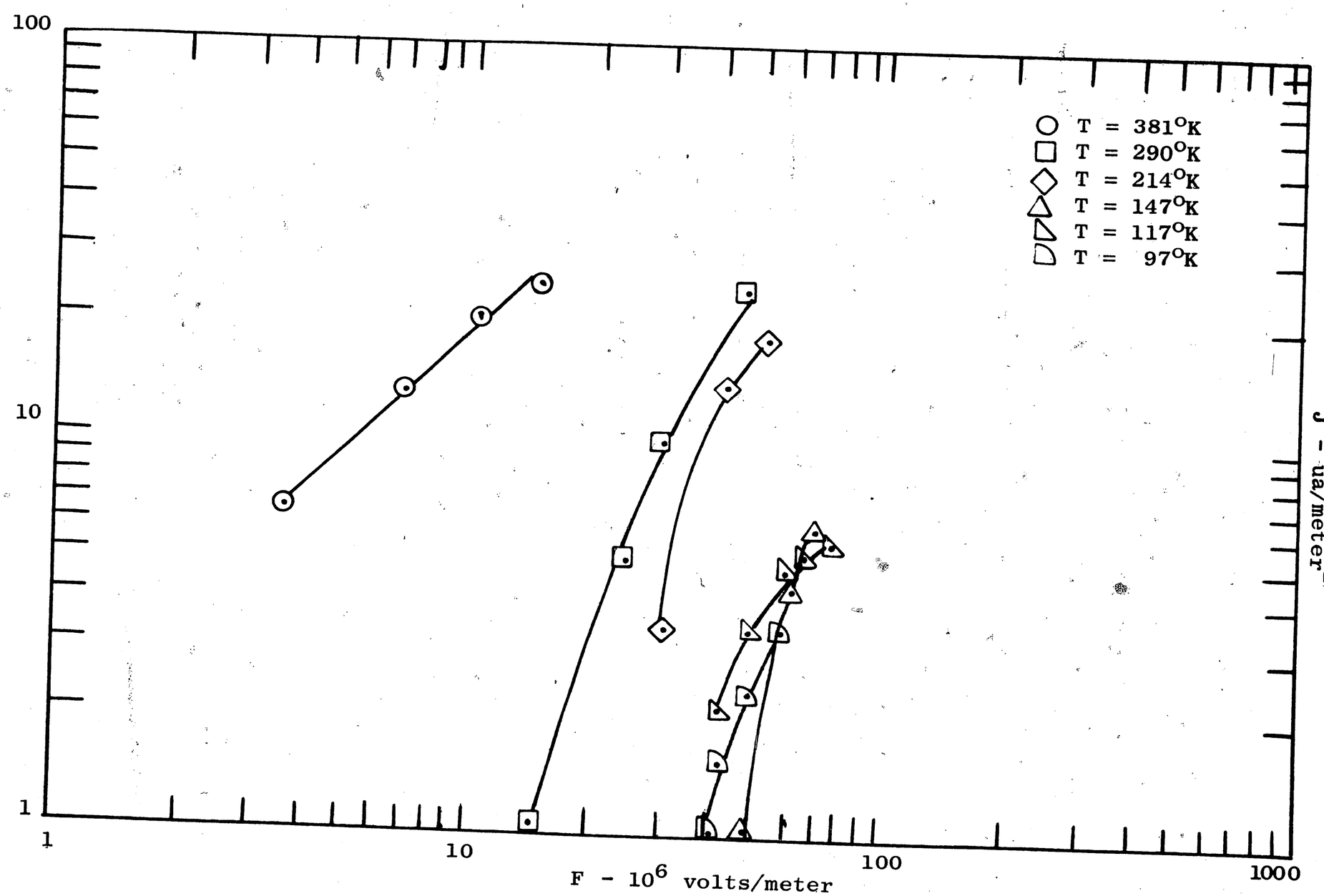

Figure 13. J vs. F for 1350 Å

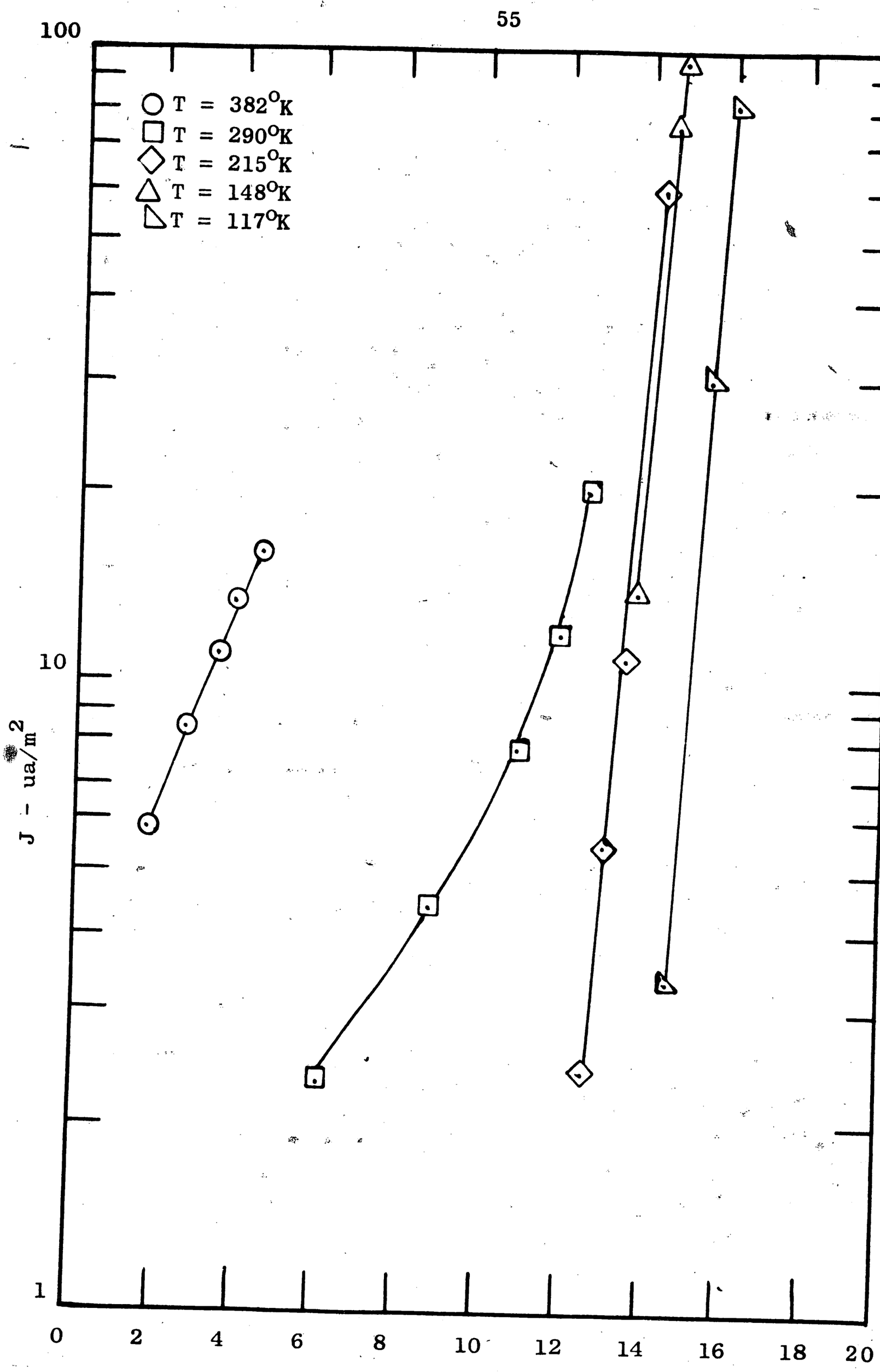

Figure 14. Schottky Plot for 50 Å

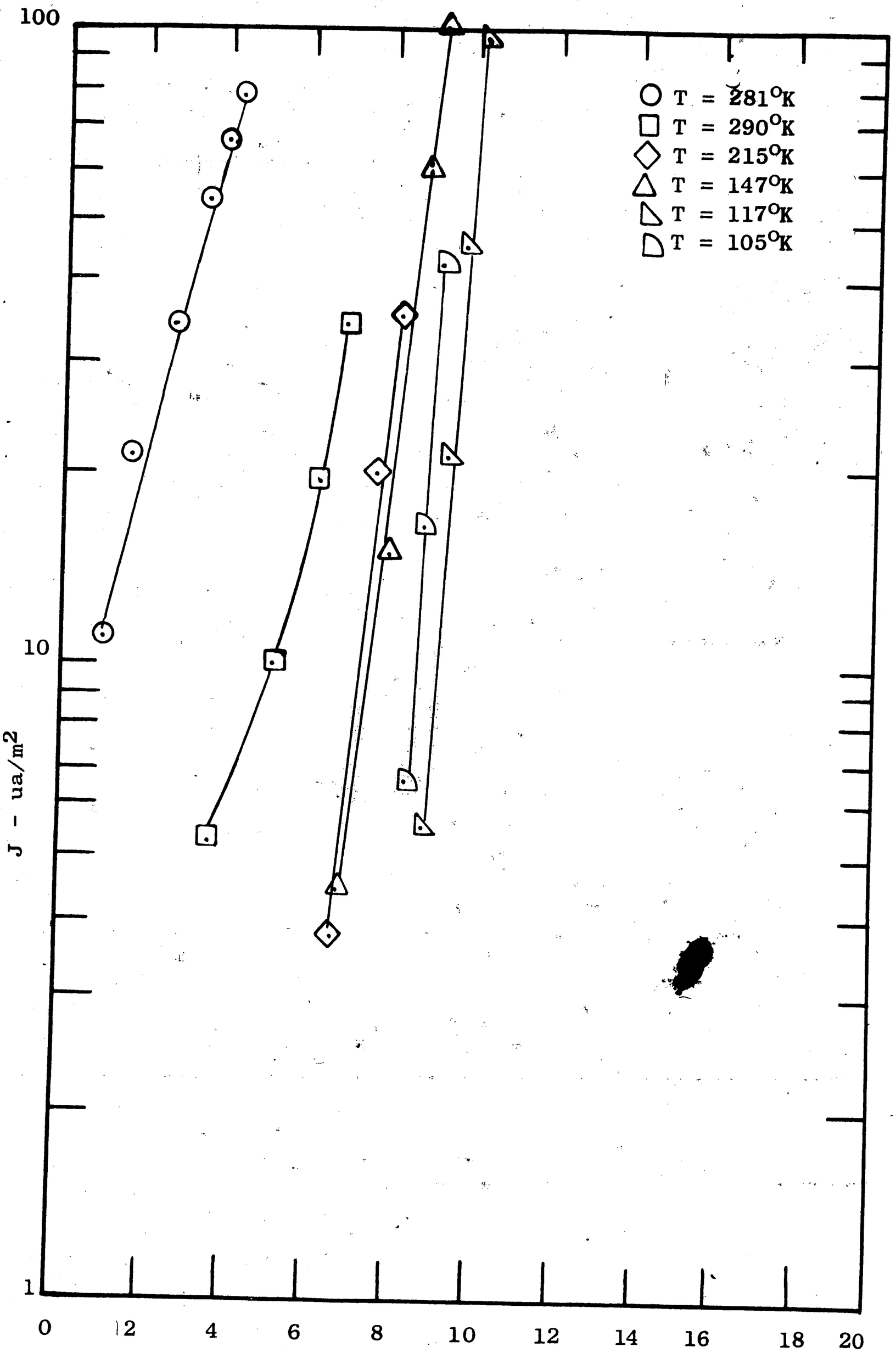

Figure 15. Schottky Plot for 150 Å

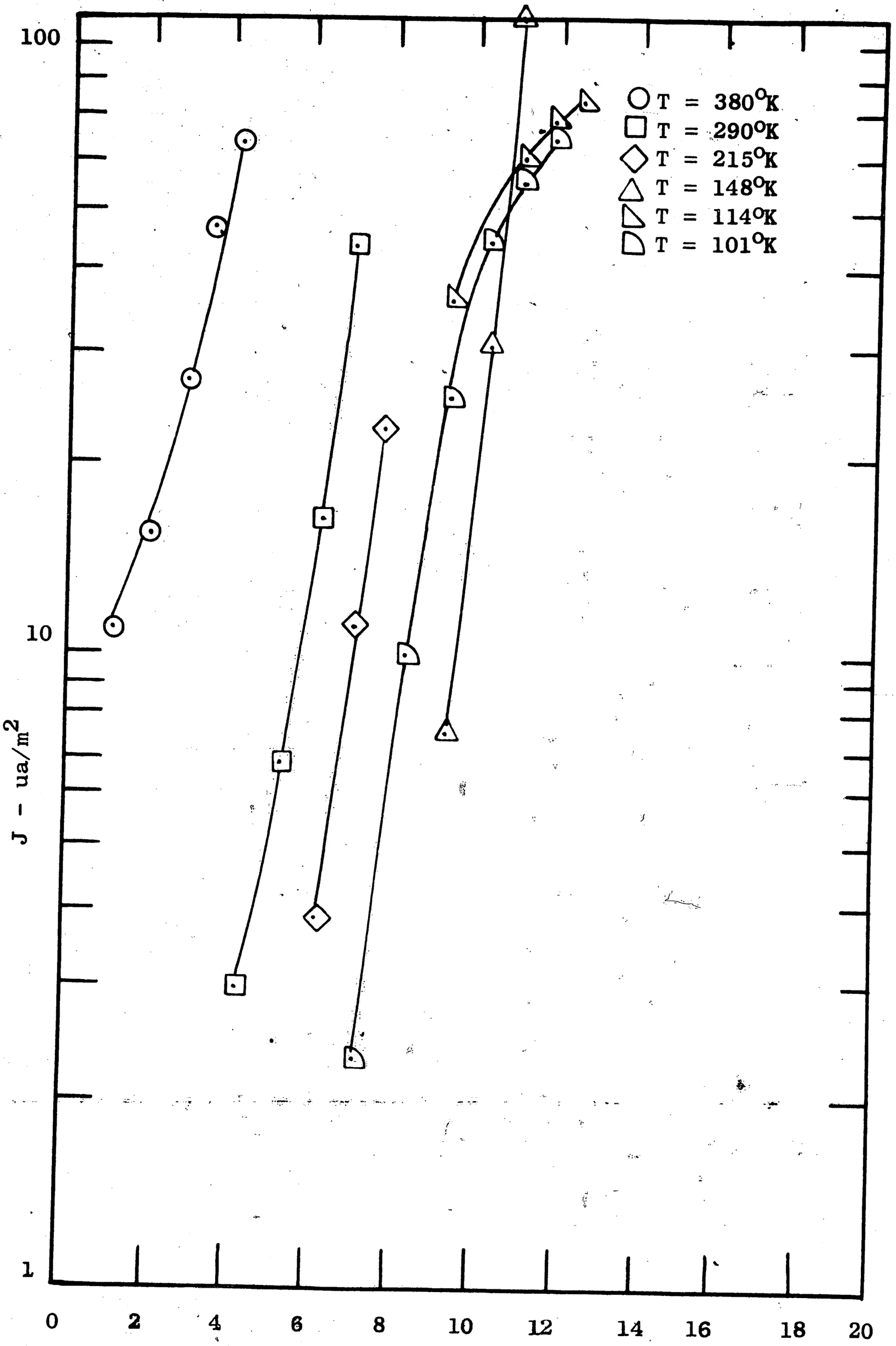

Figure 16. Schottky Plot for 450 Å

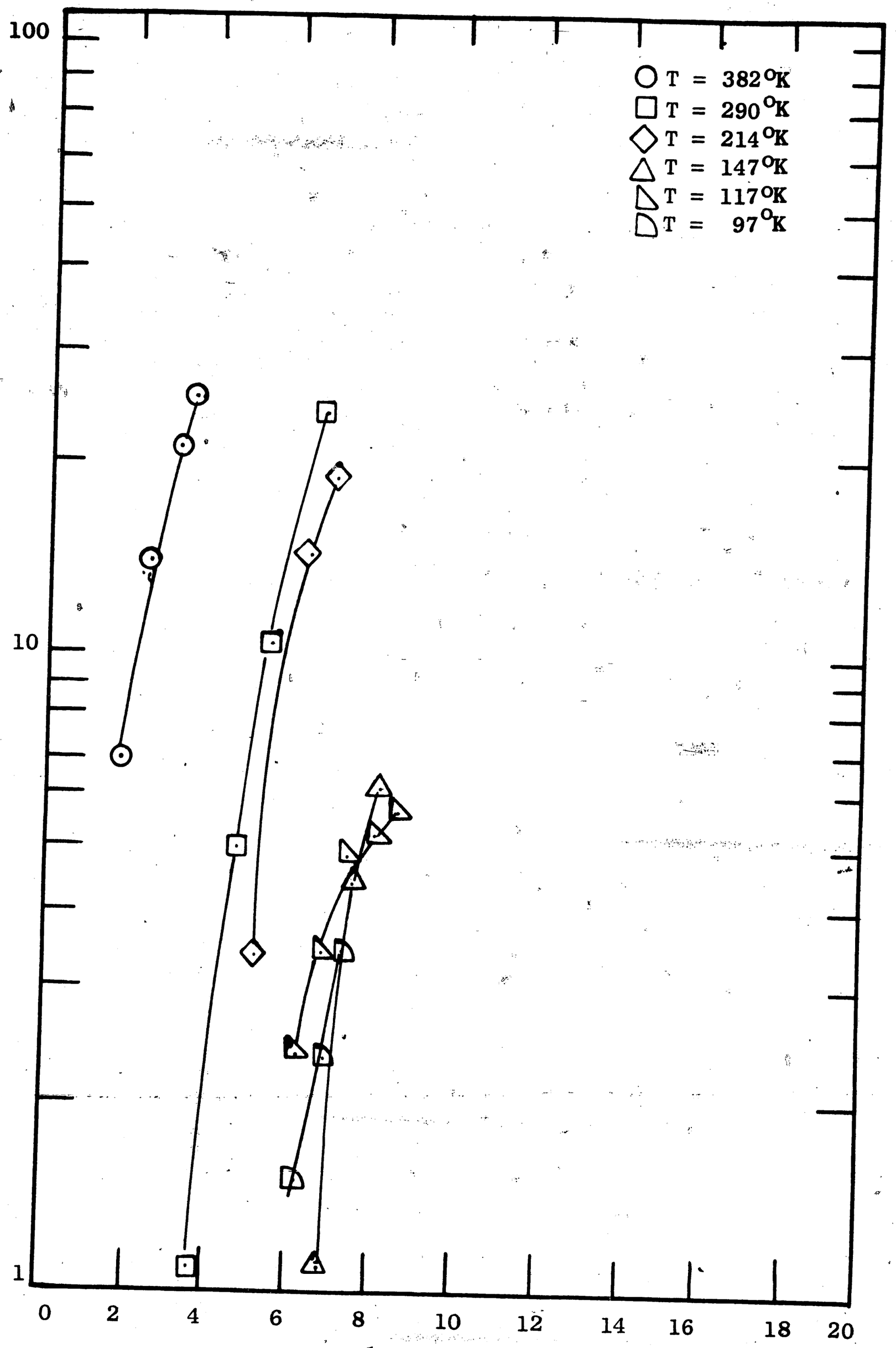

Figure 17. Schottky Plot for 1350 Å

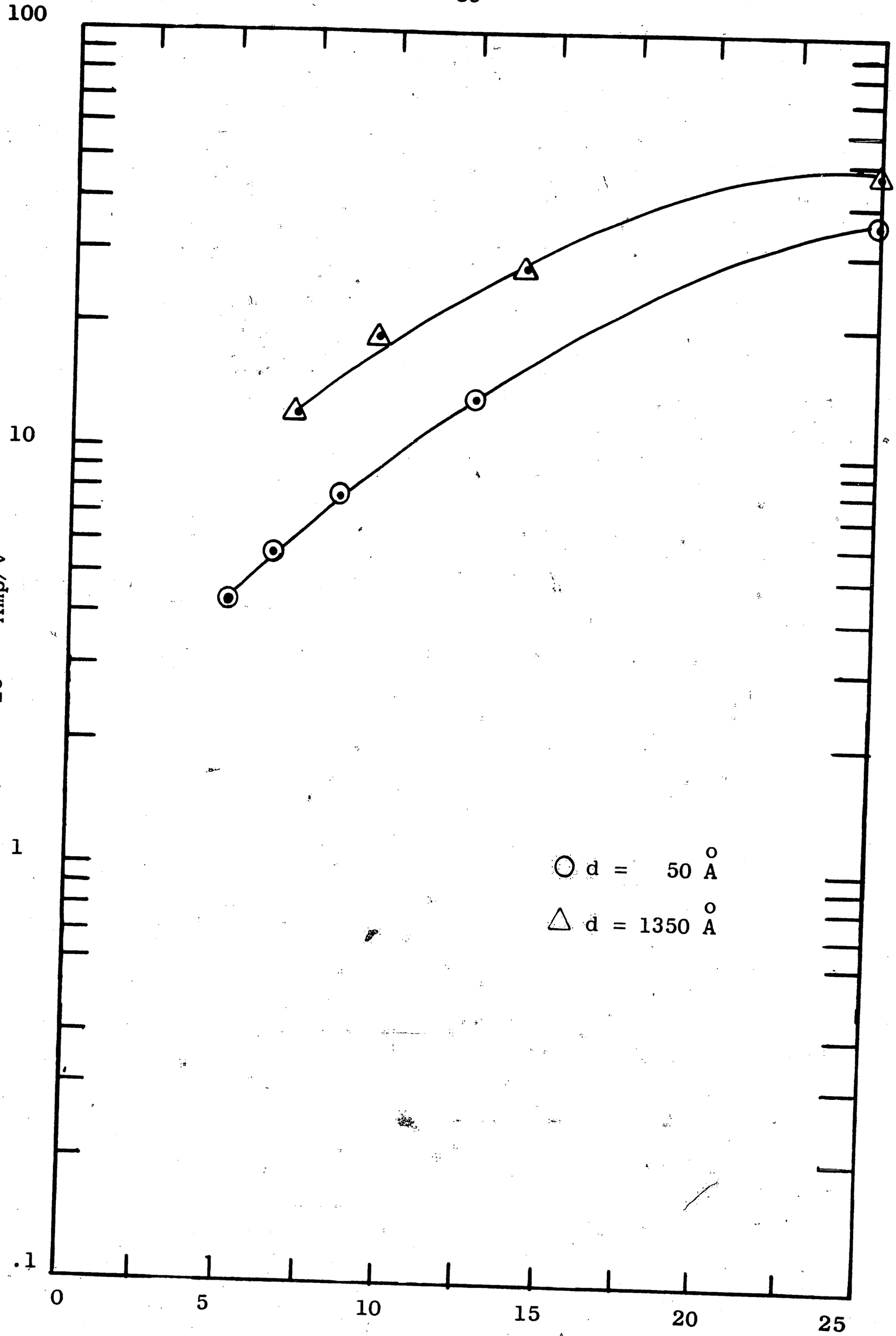

Figure 18. Fowler-Nordheim Plot for 50 Å and 1350 Å at 380°K

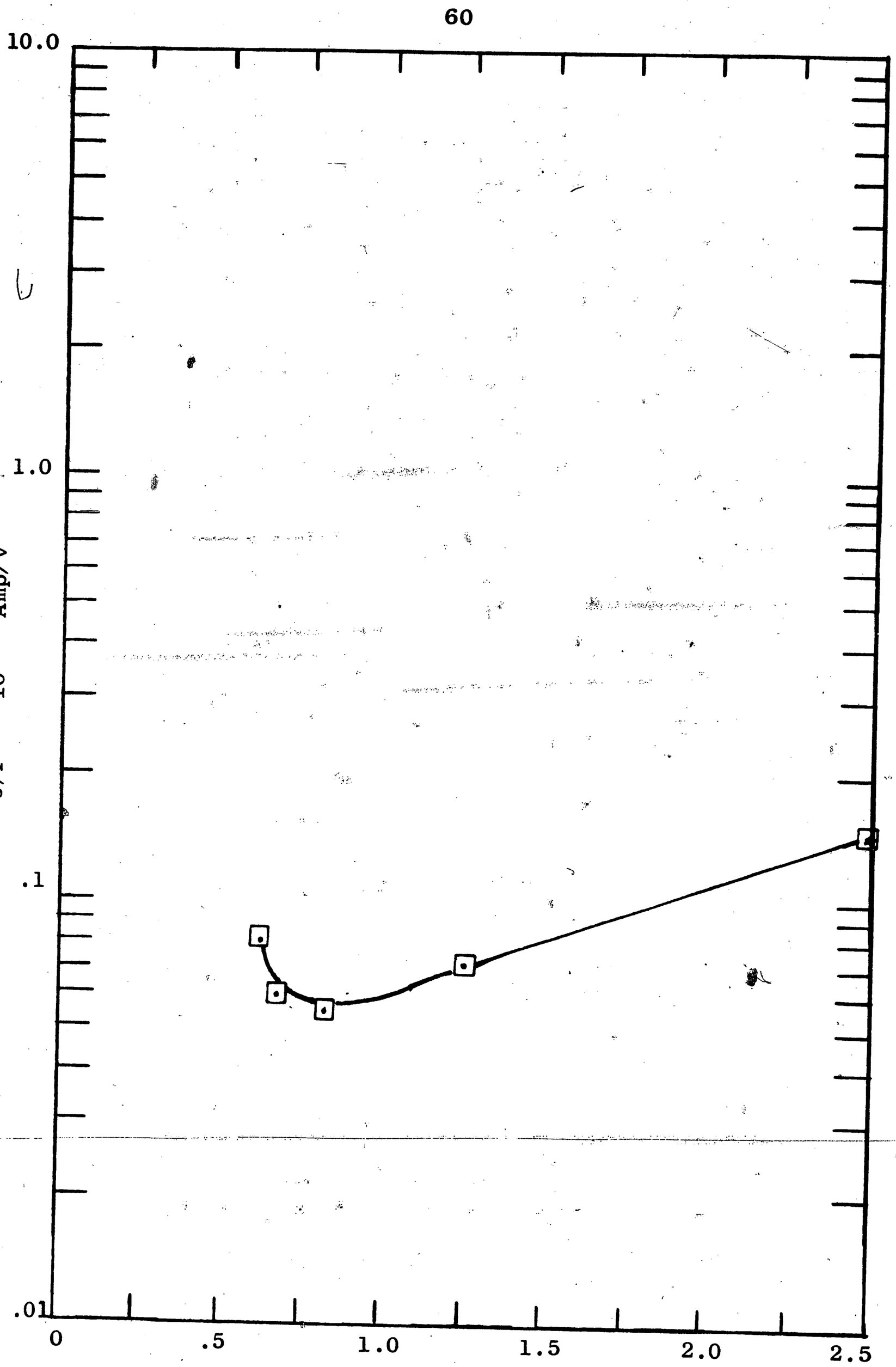

Figure 19. Fowler-Nordheim Plot for 50 Å at 290°K

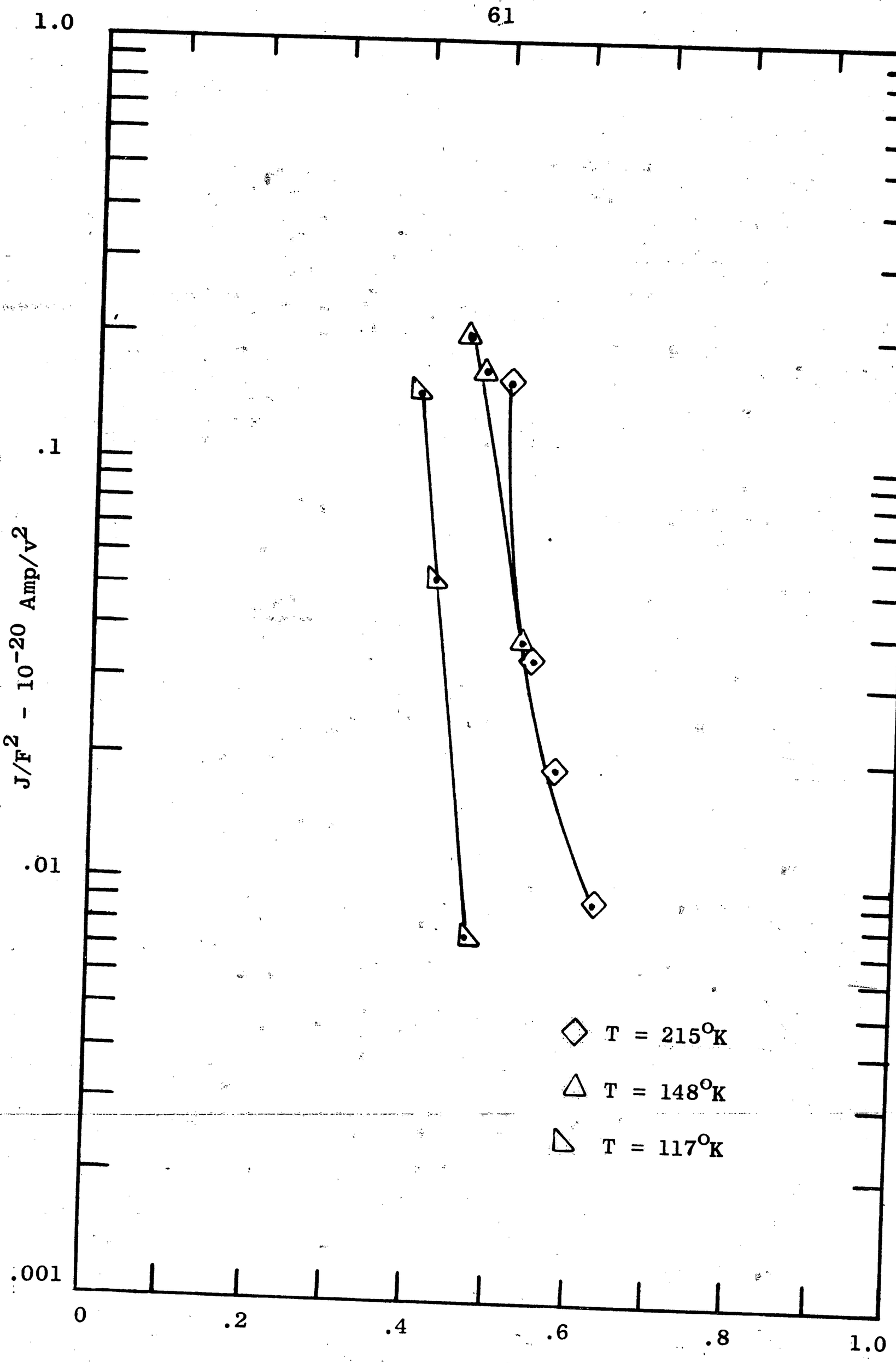

Figure 20. Fowler-Nordheim Plot for 50 Å

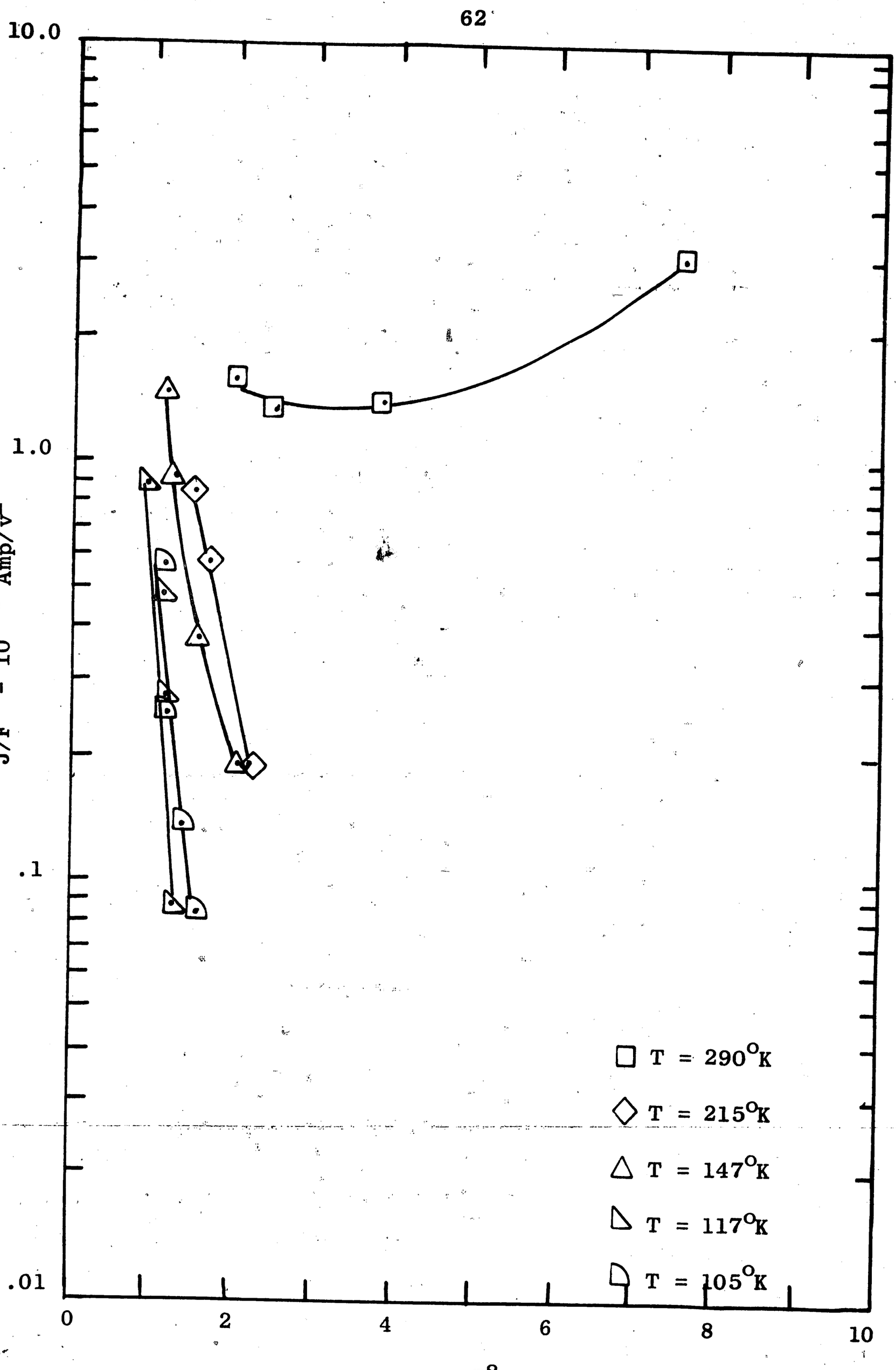

Figure 21. Fowler-Nordheim Plot for 150 Å

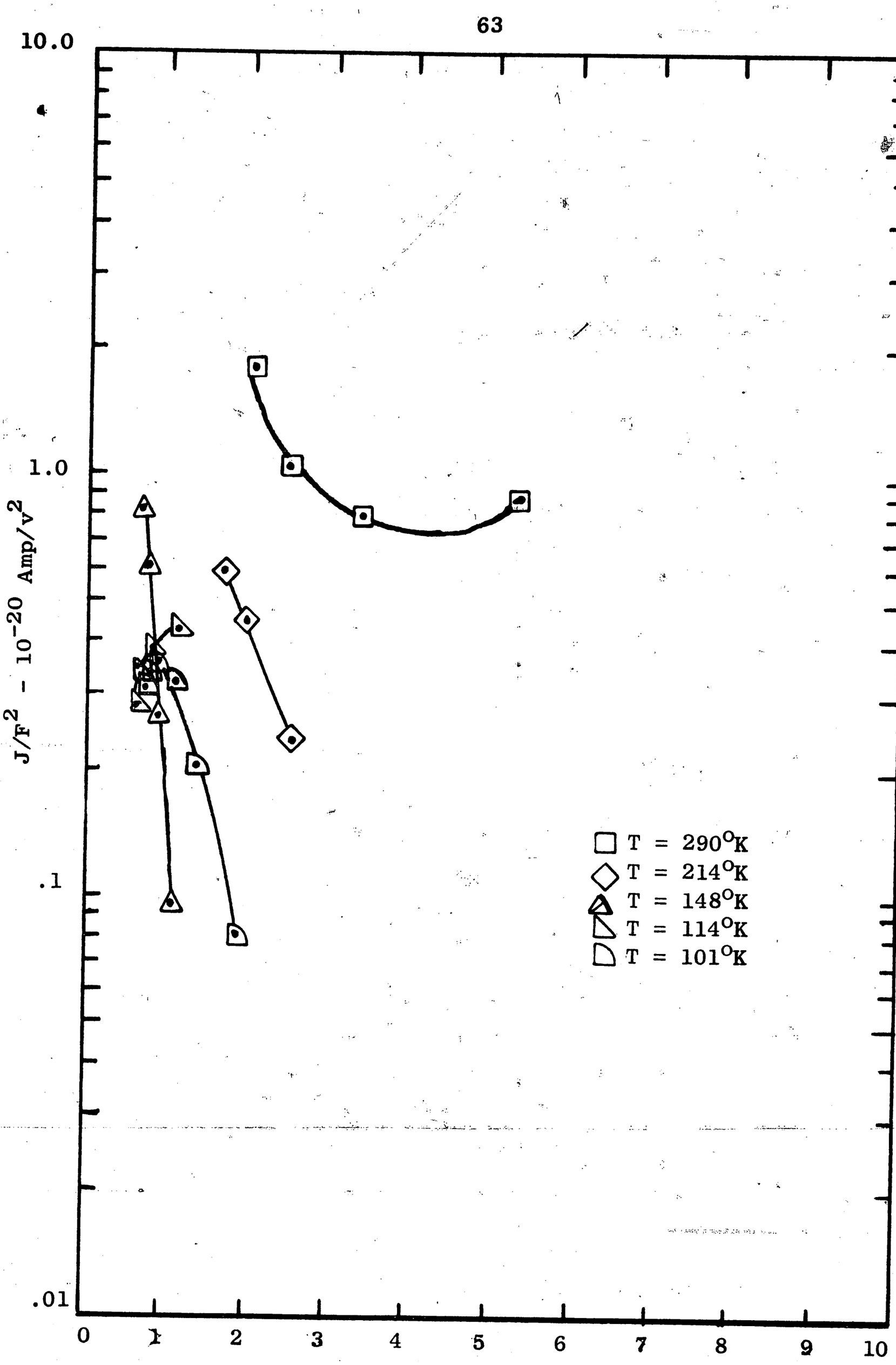

Figure 22. Fowler-Nordheim Plot for 450 Å

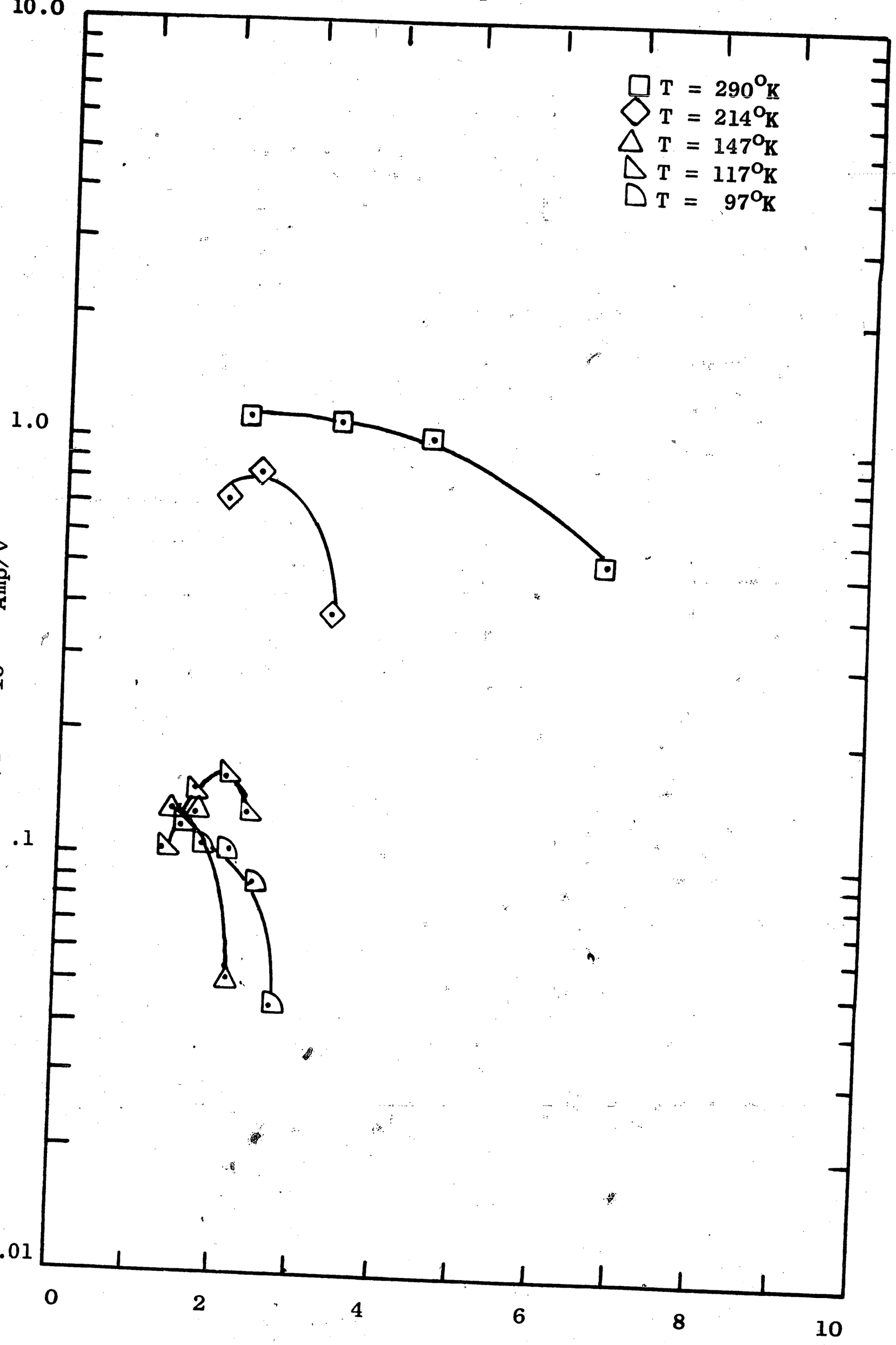

Figure 23. Fowler-Nordheim Plot for 1350 Å

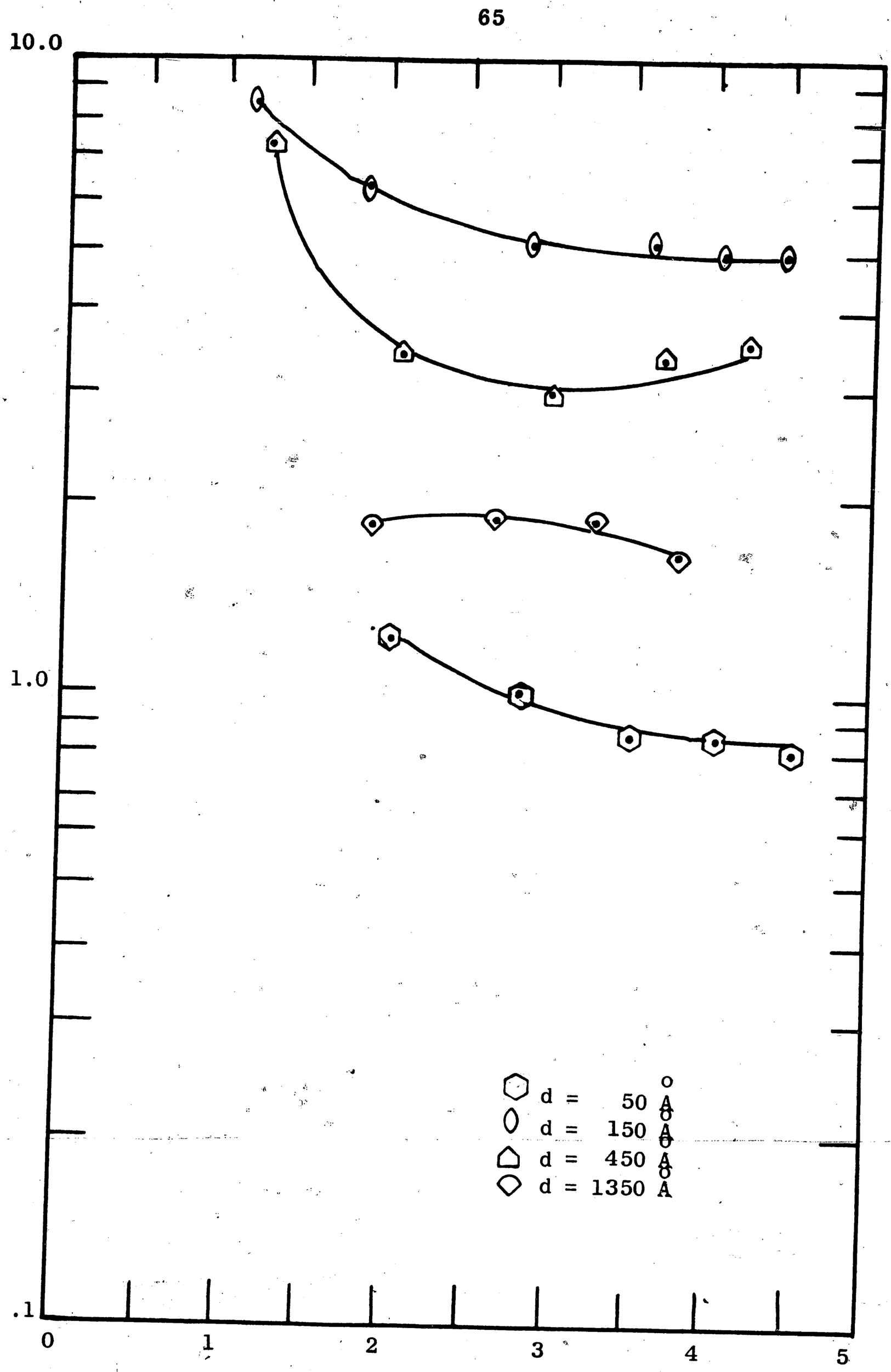

Figure 24. Plot of Data at 380°K to Mead's High Temperature Theory

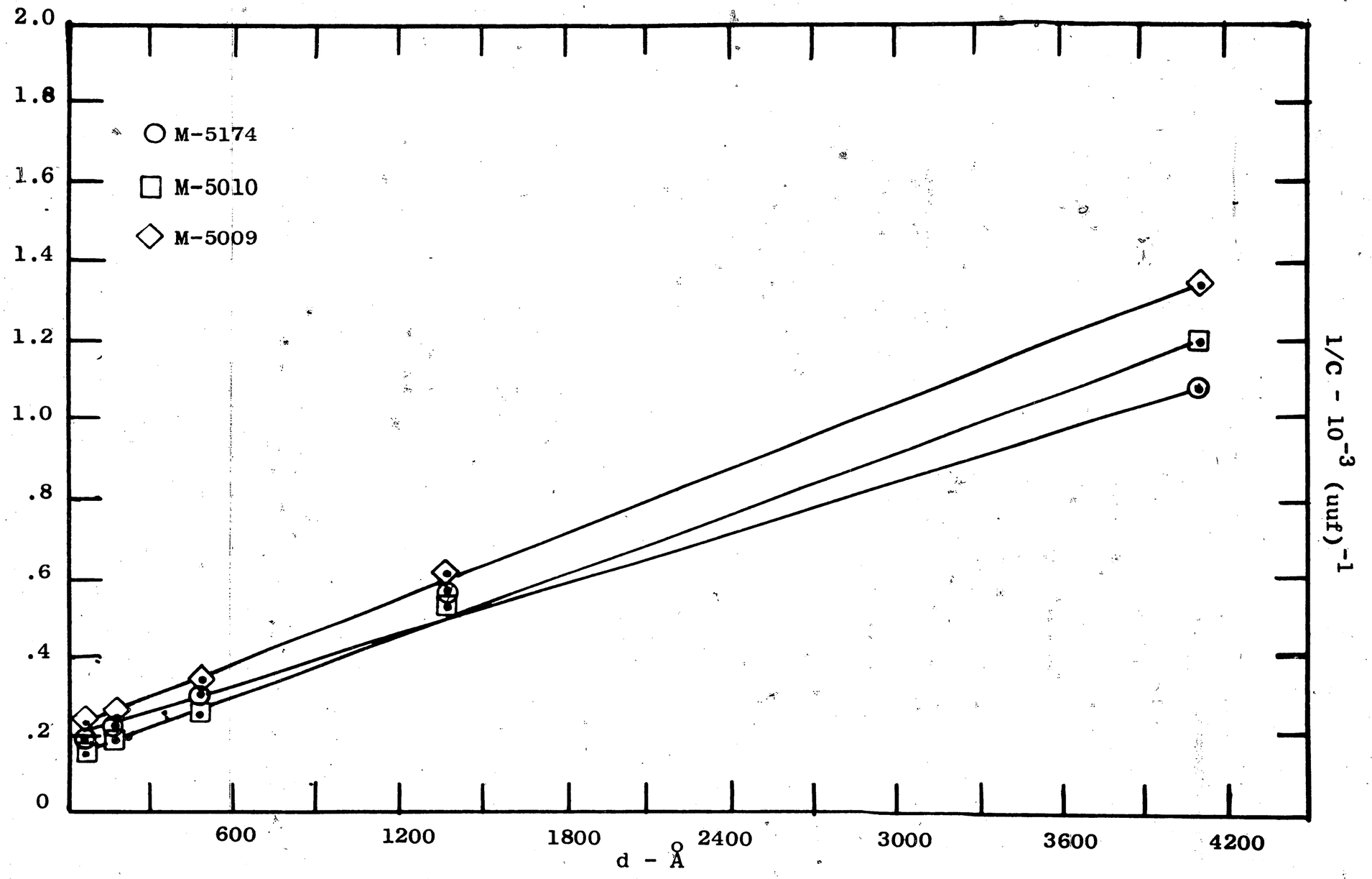

Figure 25. Anomalous Capacitance Behavior

VI. TABLE OF SYMBOLS

A = Richardson's constant or area
B = Arbitrary constant
C = Arbitrary constant or capacitance
d = Interplanar spacing of electrodes
E_c = Energy level of the conduction band
E_f = Energy of Fermi level
E_t = Energy of trap level
e = Charge of the electron
F = Field strength
F_{TFL} = Field at transition from ohmic to trap filled behavior
F_{TR} = Field at transition from ohmic to square law behavior without traps
F'_{TR} = Field at transition from ohmic to square law behavior with traps
h = Planck's constant
I = Current
J_F = Fowler-Nordheim current
J_S = Schottky current
J_{SC} = Space charge current
J_{SO} = Zero field Schottky current
J_T = Space charge current with traps distributed in energy
J_{TSC} = Space charge current with shallow traps
k = Boltzmann's constant
m = Mass of electron
N_c = Effective density of states in the conduction band
N_t = Trap density
$N_T(E)$ = Energy distribution of traps
n_c = Number of carriers in the conduction band
n_i = Number of carriers injected into the insulator due to the applied field
n_o = Equilibrium number of thermally generated carriers in the conduction band
n_t = Number of carriers in trapped states
T = Absolute temperature
$t(y)$ = A Nordheim function
V = Voltage
$v(y)$ = Nordheim's elliptic function
y = Argument of Nordheim's functions
α = Arbitrary variable
ϵ = Permittivity of material
θ = Trapping factor
μ = Mobility of charged particle
ϕ = Work function at metal-insulator interface
$\psi = E_c - E_t$

VII. BIBLIOGRAPHY

1. Mead, C.A., "Operation of Tunnel Emission Devices," Journal of Applied Physics, Vol. 32, No. 4, (April, 1961), p. 646.

2. Fisher, J.C. and I. Giaever, "Tunneling Through Thin Insulating Layers," Journal of Applied Physics, Vol. 32, No. 2, (February, 1961), p. 172.

3. Emtage, P.R. and W. Tantraporn, "Schottky Emission Through Thin Insulating Films," Physical Review Letters, Vol. 8, No. 7, (April, 1962), p. 267.

4. Standley, C.L. and L.I. Maissel, "Some Observations on Conduction Through Thin Tantalum Oxide Films," Journal of Applied Physics, Vol. 35, No. 5, (May, 1964), p. 1530.

5. Mead, C.A., "Electron Transport Mechanisms in Thin Insulating Films," Physical Review, Vol. 128, No. 5, (December, 1962), p. 2088.

6. Lampert, M.A., "Injection Currents in Insulators," Proceedings of the IRE, Vol. 50, No. 8, (August, 1962), p. 1781.

7. Rose, A., "Space Charge Limited Currents in Solids," Physical Review, Vol. 97, No. 6, (March, 1955), p. 1538.

8. Van der Ziel, A., Solid State Physical Electronics, Englewood Cliffs, N.J.: Prentice Hall, Inc., 1957.

9. Klerer, J., "Determination of the Density and Dielectric Constant of Thin Ta_2O_5 Films," Journal of Electrochemical Society, Vol. 112, No. 9, (September, 1965), p. 896.

10. Good, R.H. and E.W. Muller, "Field Emission," Handbuch der Physik, Vol. XXI, Springer Verlag, 1965, p. 176.

11. Chynoweth, A.G., "Internal Field Emission," Progress in Semiconductors, Vol. 4, (1959), p. 97.

12. Frenkel, J., "The Theory of Electric Breakdown of Dielectrics and Semiconductors," Journal of Experimental Theoretical Physics (U.S.S.R.), Vol. 8, (1938), p. 1893.

13. Young, L., Anodic Oxide Films, New York: Academic Press, 1961, p. 107.

14. Vermilyea, D.A., "The Oxidation of Tantalum at 50-300°C, Acta Met., Vol. 6, No. 3, (March, 1958), p. 166.

15. Schwartz, N. and M. Gresh, "Effect of Ambients and Contact Area on the Asymmetric Conduction of Anodic Tantalum Oxide Films," Journal of the Electrochemical Society, Vol. 112, No. 3, (March, 1965), p. 295.

16. Kittel, C., Introduction to Solid State Physics, 2nd Edition, New York: John Wiley and Sons, Inc., 1965, p. 267.

17. Murphy, E.L. and R.H. Good, "Thermionic Emission, Field Emission, and the Transition Region," Physical Review, Vol. 102, No. 6, (June, 1965), p. 1464.

18. Mead, C.A., "An Anomalous Capacitance Behavior," Physical Review Letters, Vol. 6, (1961), p. 545.

19. Namba, S., Nakajima, H. and H. Isbido, "Shottky Current Flow Through Thin Oxidized Metal Films, " Japanese Journal of Applied Physics, Vol. 32, No. 8, (1963), p. 562.

VIII. VITA

R. A. Rodriguez, Jr., was born in Raleigh, N. C., on December 5, 1931. He attended various public grade schools in Johnstown, Pa.; Pine Bluff, Ark.; Temple, Texas; and Igloo, S. D. He attended public high schools in Igloo, S. D; Greensboro, N. C.; and Johnstown, Pa., and was graduated from Westmont High School in 1949.

The author entered Pennsylvania State University and was awarded a Bachelor of Science degree in Electrical Engineering in January, 1956.

He was elected to membership in the following honorary faternities: Phi Eta Sigma, Tau Beta Pi, Sigma Tau, and Eta Kappa Nu.

Upon graduation the author accepted a position with Western Electric Co., at Winston-Salem, North Carolina. He worked as a test planning engineer designing test equipment and procedures for various guided missile systems, Navy fire control systems, and BMEWS. In February, 1962, he was transferred to the staff of the Graduate Engineering Training Center at Winston-Salem as a Section Chief. There he taught courses in electronics, semiconductor device theory, semiconductor device application, switching circuits, programming, and computer design.

In June, 1964, he was promoted to Senior Research Engineer and accepted into the Lehigh Masters Program at the Engineering Research Center at Princeton, New Jersey.